Naval Research Laboratory
Washington, DC 20375-5320

NRL/MR/7225--93-7346

Surface and Internal Signatures of Organized Vortex Motions in Stratified Fluid

Y. T. Fung
S. W. Chang

Remote Sensing Physics Branch
Remote Sensing Division

July 15, 1993

REPORT DOCUMENTATION PAGE

Form Approved
OMB No. 0704-0188

1. AGENCY USE ONLY (*Leave Blank*)	2. REPORT DATE	3. REPORT TYPE AND DATES COVERED
	July 15, 1993	

4. TITLE AND SUBTITLE

Surface and Internal Signatures of Organized Vortex Motions in Stratified Fluid

5. FUNDING NUMBERS

PE - 61153N 33
PR - RR033-02042
WU - 364803

6. AUTHOR(S)

Y.T. Fung and S.W. Chang

7. PERFORMING ORGANIZATION NAME(S) AND ADDRESS(ES)

Naval Research Laboratory
Washington, DC 20375-5320

8. PERFORMING ORGANIZATION REPORT NUMBER

NRL/MR/7225-93-7346

9. SPONSORING/MONITORING AGENCY NAME(S) AND ADDRESS(ES)

Office of Naval Research
Arlington, VA 22217-5660

10. SPONSORING/MONITORING AGENCY REPORT NUMBER

11. SUPPLEMENTARY NOTES

12a. DISTRIBUTION/AVAILABILITY STATEMENT

Approved for public release; distribution unlimited.

12b. DISTRIBUTION CODE

13. ABSTRACT (*Maximum 200 words*)

Internal vortex patterns and the corresponding free surface signatures generated by a submerged sphere moving in a stratified fluid are numerically simulated by a three-dimensional time-dependent computer model. The flow is assumed to be incompressible and hydrostatic, and the Boussinesq approximation is applied. The turbulent mixing is modeled using the Smagorinsky formula for horizontal fluxes and a Richardson number closure for vertical fluxes. The numerical techniques include a second-order finite difference scheme with a staggered and stretched grid system. To efficiently handle the slow baroclinic and the fast barotropic modes in the flow, a split-explicit method is used to separately integrate the two modes in time. This method allows us to economically simulate the time history of the slowly evolving vortices.

Preliminary results for the velocity field, the flow pattern, the density distribution, and the induced surface signature are presented. They consistently reveal the existence of coherent structures in the stratified flow field.

A mechanism based on the interaction of the wake vorticity and the buoyancy induced oscillation is proposed for the generation and growth of the horizontal vortices in stratified fluids. This mechanism explains why the horizontal vortices appear long after the initial disturbances generated by a submerged moving body have dissipated, and why these vortices exist only in stratified fluids but not in homogenous media.

In a forthcoming paper, we will examine how the density distribution, the depth of the moving object, and the depth of the channel floor affect the organized vortex structures and the corresponding surface signatures.

14. SUBJECT TERMS

15. NUMBER OF PAGES

51

16. PRICE CODE

17. SECURITY CLASSIFICATION OF REPORT	18. SECURITY CLASSIFICATION OF THIS PAGE	19. SECURITY CLASSIFICATION OF ABSTRACT	20. LIMITATION OF ABSTRACT
UNCLASSIFIED	UNCLASSIFIED	UNCLASSIFIED	UL

CONTENTS

SURFACE AND INTERNAL SIGNATURES OF ORGANIZED VORTEX MOTIONS IN STRATIFIED FLUID

1. Introduction

Organized vortices form in nature. The formation of wake vortices in the stratified atmosphere and ocean has been observed (Chopra & Hubert 1965, Lyons & Fujita 1968, Pao & Kao 1976, Thomson *et al* 1977), analyzed (e.g., Chopra 1973), and reproduced in laboratories (Barnett 1972, Pao & Kao 1977). The atmosphere vortices, normally identified by the shallow stratocumulus clouds below a capping inversion, form when obstacles (such as island mountains) are higher than the inversion with a large-scale parallel wind in the lower atmosphere.

Coherent structures in stratified fluids, especially solitary waves produced by the collapse of a mixed region of fluid (Wu 1969, Kao & Pao 1979), and horizontal vortices evolving in the late wakes of a submerged moving object (Pao & Kao 1977, Lin & Pao 1979), have puzzled many researchers because of the striking phenomena these flows reveal and their distinct characteristic difference from those in homogenous fluids. The puzzling stems from at least two reasons. First, the coherent structures that are intrinsic in internal waves or wakes exist only in a stratified environment but not in a homogeneous one. Second, flow structures in internal waves or wakes dissipate very slowly. Once generated they either propagate very long distance or persist very long time.

Density inhomogeneity and gravity play a very subtle role in the dynamics of stratified fluid motions. Density inhomogeneity by itself has very minor effects on flows. Neither does gravity have influence on fluid flows in a homogeneous medium. The presence of the inhomogeneity, however, allows gravity to play a role in the dynamics of fluid motions. Theoretically speaking, the interaction of the density inhomogeneity with gravity or with other force fields is present as a second order singularity in the equations for flow stability, and therefore, can not be ignored no matter how small the density inhomogeneity is (Mile 1961, Howard 1961, Fung & Kurzweg 1975). Such interaction produces an oscillation mechanism that dominates the motion of the coherent structures in an inhomogeneous environment. This the why the very weakly stratified atmosphere and ocean can support internal waves, wakes, and other organized flow structures that do not exist in a homogeneous environment.

Manuscript approved April 28, 1993.

Vortex motions in a gravity-stratified fluid are further complicated by three other factors; the centrifugal force field generated by the rotation of the flow, the radial density gradient induced by the pressure constraint, and the interaction of the two force fields with the density inhomogeneities in both the gravitational and centrifugal directions.

The rotation of vortices plays a dual role in the stability of the organized flow structures. While the angular velocity gradient produces shear effects which always destabilize the flow, the angular velocity itself, interacting with the density inhomogeneity, creates a centrifugal force field that can either stabilize or destabilize the flow field (Fung 1983).

As required by the balance of pressure in all directions, the angular velocity of vortex motions automatically induces density gradients in the radial direction. This induced density gradient allows the centrifugal force to play a role in the dynamics of the flow structures similar to what the gravity-stratified density gradient does in the gravitational force field, and becomes another driving force for the motion of the coherent structures in a stratified environment.

As a result of the above interactions of the force fields and density inhomogeneities in more than one direction, any organized flow structures, if existing, will have to satisfy all the required conditions. This includes the stability condition in the gravitational direction, the stability condition in the centrifugal direction, and the pressure balance condition imposed by the pressure constraint (Fung 1986, 1991).

The presence of free surface in vortex motions in a stratified fluid even further complicates the already complex dynamic system. The barotropic mode prompted by the free surface is fast moving and must be treated numerically for computational stability. To efficiently handle this fast moving mode, a split-explicit numerical scheme (Chang 1984, 1985) was used to separately integrate different modes in the ocean. In addition to this barotropic mode, the change of the surface height also complicates the balance of the centrifugal and gravitational forces and thus their interaction with density distribution. Besides, the perturbation of the free surface hight is difficult to observe and measure both in laboratories and over the ocean, and thus further hampers the understanding of the phenomenon.

As observed by Pao & Kao (1977) in their laboratory experiment, when a sphere is towed through a stratified fluid, vortices are first shed without any preference in direction. The region immediately behind the towed body is in a turbulent state with a considerable amount of mixing. This state of turbulence is quickly inhibited by the density stratification in the vertical direction. The mean motion in the horizontal direction then dominates the wake. The flow first meanders and then gradually rolls up into vortices. The resultant pattern formed in the late wake, even though inherently three-dimensional, is confined within a relatively thin horizontal layer, and is reminiscent of the two dimensional Kármán vortex street if observed from the gravitational direction.

Most of the modelling of wake vortices are conducted with a two-dimensional model (e.g., Karniadakis & Triantafyllou 1989) in which the effects of stratification and horizontal mass divergence are not properly considered. The wake vortices generated in such a model, though appear like the Kámán vortex streets, may have a completely different mechanism of formation. As will be discussed in Section 5 of this paper, no corresponding two-dimensional model can adequately describe the horizontal vortices in stratified fluids because the stratification can not be properly parameterized.

This paper will (1) briefly describes a three-dimensional numerical model with a free surface that is capable of generating the vortex motion behind a submerged moving body or other organized flow structures in a stratified environment; and (2) propose, based on the numerical results obtained, a mechanism for the generation and growth of horizontal vortices in stratified fluids. It is not our intention to realistically simulate the detailed flow structure near a submerged moving body. Instead, our interest is the development of organized flow structures after the initial wake turbulence induced by submerged moving objects has dissipated. We have limited the scope of this paper to the generation and growth of organized flow structures in the stratified late wake. Specifically, Section 2 will present the formulation of model dynamics, turbulent mixing, mode splitting, and numerical techniques. Section 3 will describe the near field velocity profile to generate the horizontal vortices. Section 4 will discuss the p minary results of such vortices and examine the relationship between the flow structure and the induced free surface signature.

Section 5 will present a mechanism for the generation and evolution of horizontal vortices based on the numerical results. Section 6 will conclude our findings.

2. The 3D Numerical Model

A three-dimensional time-dependent nonlinear model is constructed to study the wake vortices in a stratified fluid. The flow is assumed to be incompressible and hydrostatic. The Boussinesq approximation is applied. The governing equations, the turbulent closures, the splitting of barotropic and baroclinic modes, the grid structure, the boundary and initial conditions of the model will be discussed in this section. The model describes the motion of a stratified fluid in a tank-like confine in the Cartesian coordinates with a flat rigid bottom, a free surface, and close or open side walls. The x-direction is the direction of towing, the y-direction is cross-stream, and the z-direction is vertical and opposite to the gravity. As shown by Figure 1, the fluid in the model has an average height of H with a free surface perturbation h such that $h << H$.

a. Governing Equations

The horizontal equations of motion in the x- and y-directions of the model are

$$\frac{\partial u}{\partial t} + u\frac{\partial u}{\partial x} + v\frac{\partial u}{\partial y} + w\frac{\partial u}{\partial z} = -\frac{1}{\rho_o}\frac{\partial p}{\partial x} + F_h(u) + F_z(u) \tag{1}$$

$$\frac{\partial v}{\partial t} + u\frac{\partial v}{\partial x} + v\frac{\partial v}{\partial y} + w\frac{\partial v}{\partial z} = -\frac{1}{\rho_o}\frac{\partial p}{\partial y} + F_h(v) + F_z(v) \tag{2}$$

Here u, v, and w are velocity components in the x, y, and z directions, respectively, and ρ_o is a density constant. Functions F_h and F_z represent the effects of turbulent mixing from the horizontal and vertical fluxes. The equation of motion in z-direction, under the hydrostatic assumption, is reduced to

$$\frac{\partial p}{\partial z} = -\rho g \tag{3}$$

where ρ is the density of the fluid. For the far-field simulation as in the present case, organized vortices form long after the initial disturbances generated by the moving object have dissipated. The hydrostatic assumption is justified at this stage when the buoyancy effect due to density stratification dominates the vertical motion. The mass conservation of the model is

$$\frac{\partial \rho}{\partial t} + u\frac{\partial \rho}{\partial x} + v\frac{\partial \rho}{\partial y} + w\frac{\partial \rho}{\partial z} = F_h(\rho) + F_z(\rho) \tag{4}$$

For incompressible fluids, the continuity equation is

$$\frac{\partial u}{\partial x} + \frac{\partial v}{\partial y} + \frac{\partial w}{\partial z} = 0 \tag{5}$$

With the rigid bottom where the vertical velocity vanishes, i.e., $w = 0$ at $z = 0$, an vertical integration of (5) from the bottom to the surface of the fluid ($z = H + h$) yields

$$\int_o^{H+h} \frac{\partial w}{\partial z} dz = w(H+h) - w(0) = w(H+h)$$

$$= -\int_o^{H+h} (\frac{\partial u}{\partial x} + \frac{\partial v}{\partial y}) dz = H(\frac{\partial \langle u \rangle}{\partial x} + \frac{\partial \langle v \rangle}{\partial y}) + h(\frac{\partial u_s}{\partial x} + \frac{\partial v_s}{\partial y})$$

where h is the surface height perturbation and the depth average $\langle \phi \rangle$ of any function ϕ is defined as

$$\langle \phi \rangle = \int_o^H \phi dz \tag{6}$$

where

$$\phi = \phi' + \langle \phi \rangle \tag{7}$$

The prognostic equation for the surface height perturbation h, after rearranging, is obtained as

$$\frac{\partial h}{\partial t} = -H\left(\frac{\partial u}{\partial x} + \frac{\partial v}{\partial y}\right) - \left[\frac{\partial}{\partial x}(hu_s) + \frac{\partial}{\partial y}(hv_s)\right] \tag{8}$$

where u_s and v_s are surface current velocities with negligible variations across h.

b. Turbulence Mixing

There are many ways to model the turbulent mixing. The available parameterizations vary from the simple K-theory with a constant diffusion coefficient to higher order turbulent closures. Direct numerical simulations require no parameterization but demand much more time and capability in computing. To simplify the computation, we opt for a somewhat conservative turbulent closure just enough for the model to form vortices.

For the horizontal diffusion, Smagorinsky's formula is used to accept contribution from the rate of deformation of fluid elements as follows :

$$K_h = \frac{\kappa^2}{2}\Delta x \Delta y \sqrt{D_1^2 + D_2^2} \tag{9}$$

Here κ is the von Kármán constant, Δx and Δy are grid sizes, and the deformation fields are defined as

$$D_1 = \frac{\partial u}{\partial x} - \frac{\partial v}{\partial y}, \qquad D_2 = \frac{\partial v}{\partial x} + \frac{\partial u}{\partial y} \tag{10}$$

The horizontal turbulent mixing function in (1) and (2) is then defined as

$$F_h(u, v, \rho) = \frac{\partial}{\partial x}\left[K_h \frac{\partial(u, v, \rho)}{\partial x}\right] + \frac{\partial}{\partial y}\left[K_h \frac{\partial(u, v, \rho)}{\partial y}\right] \tag{11}$$

For the vertical diffusion, a Richardson number closure is used to admit influence from both the vertical shear and the density stratification. The vertical diffusion coefficient is defined as

$$K_v = (\Delta z)^2 \sqrt{\left[(\frac{\partial u}{\partial z})^2 + (\frac{\partial v}{\partial z})^2\right](1 - R_i)}, \qquad \text{for} \qquad 1 > R_i > 0. \tag{12}$$

where the Richardson number is defined as

$$R_i = \frac{N^2}{(\frac{\partial u}{\partial z})^2 + (\frac{\partial v}{\partial z})^2}$$

and the Brunt-Väisälä frequency is defined as

$$N^2 = -\frac{g}{\rho}\frac{\partial \rho}{\partial z}. \tag{13}$$

The vertical mixing vanishes as the gradient Richardson number equals to or larger than unity. The vertical turbulent mixing function in (1) and (2) then defined as

$$F_z(u, v, \rho) = \frac{\partial}{\partial z}\left[K_v \frac{\partial (u, v, \rho)}{\partial z}\right]. \tag{14}$$

c. Splitting of Internal and External Modes

The governing equations (1) to (5) and (8) contain the internal gravity (baroclinic) and external gravity (barotropic) modes. For a certain depth and density stratification in the ocean or in wave tanks, the characteristic phase speed of the external gravity mode $c = \sqrt{gH}$ is about one or two orders of magnitude larger than the first internal gravity mode. In various configurations of our model, the average depth H ranges from 30 to 70 cm, giving a phase speed of 171 to 262 cm/sec for the external modes. The maximum internal phase speed, however, is dictated by the towing speed, which is 4 cm/sec. It is expedient to separate the governing equations into a barotropic part and a baroclinic part and to numerically integrate them at different time intervals to achieve computational efficiency (Chang 1984, 1985).

Now we rewrite (1) and (2) as

$$\frac{\partial u}{\partial t} = A - \frac{1}{\rho_o}\frac{\partial p}{\partial x} \tag{15}$$

$$\frac{\partial v}{\partial t} = B - \frac{1}{\rho_o}\frac{\partial p}{\partial y} \tag{16}$$

where

$$A = -u\frac{\partial u}{\partial x} - v\frac{\partial u}{\partial y} - w\frac{\partial u}{\partial z} + F_h(u) + F_z(u)$$

$$B = -u\frac{\partial v}{\partial x} - v\frac{\partial v}{\partial y} - w\frac{\partial v}{\partial z} + F_h(v) + F_z(v)$$

For any point in the fluid at the depth of $H + h - z$, the total pressure is equal to

$$p(z) = g\int_z^{H+h} \rho dz' = g\int_z^{H} \rho dz' + g\int_H^{H+h} \rho dz' \tag{17}$$

The value of $p(z)$ in (17) contains a large portion of static pressure $\rho_o g(H - z)$ which does not contribute to the dynamics of the motion. Defining a reference pressure

$$p_r(z) = p(z) - \rho_o g(H - z)$$

and substituting into (17), we have

$$p_r(z) = g\int_z^{H} \epsilon' dz' + g\langle\epsilon\rangle(H - z) + (\rho_s - \rho_o)gh, \tag{18}$$

where ρ_s is the fluid density at the free surface, $\epsilon = \rho - \rho_o$ the density deviation, $\langle\epsilon\rangle$ the depth average of ϵ as defined in (6), and $\epsilon' = \epsilon - \langle\epsilon\rangle$ as in (7). To arrive in (18) we have assumed that the density variation across h is negligible.

The second term in (18) is the static pressure produced by the depth average density variations in stratified fluids. The last term in (18) contains the contribution from the perturbation of the free surface, a depth-independent pressure force exerting on the fluid. Depth averaging (18) yields the depth average reference pressure and its deviation as :

$$\langle p_r \rangle = \frac{1}{2}\langle \epsilon \rangle gh + g\langle \epsilon' \rangle + (\rho_s - \rho_o)gh, \tag{19}$$

and

$$p'_r = p_r - \langle p_r \rangle. \tag{20}$$

The depth average pressure gradient force, $\nabla\langle p_r \rangle$, exerts uniformly throughout the fluid column and excites the barotropic mode in the fluid. The deviation of the pressure gradient force, on the other hand, excites only the baroclinic mode and contributes more to the detailed internal structures of the organized vortex motion. Taking the depth average of (11) and (12), we separate the prognostic equations (1) and (2) into the barotropic set

$$\frac{\partial \langle u \rangle}{\partial t} = \langle A \rangle - \frac{1}{\rho_o}\frac{\partial \langle p_r \rangle}{\partial x}, \tag{21}$$

$$\frac{\partial \langle v \rangle}{\partial t} = \langle B \rangle - \frac{1}{\rho_o}\frac{\partial \langle p_r \rangle}{\partial y}. \tag{22}$$

and the baroclinic set

$$\frac{\partial u'}{\partial t} = A' - \frac{1}{\rho_o}\frac{\partial p'_r}{\partial x}, \tag{23}$$

$$\frac{\partial v'}{\partial t} = B' - \frac{1}{\rho_o}\frac{\partial p'_r}{\partial y}, \tag{24}$$

$$\frac{\partial \epsilon'}{\partial t} = -u\frac{\partial \epsilon'}{\partial x} - v\frac{\partial \epsilon'}{\partial y} - w\frac{\partial \epsilon'}{\partial z} + F_h(\epsilon) + F_z(\epsilon). \tag{25}$$

One can of course further separate the internal modes such as in Madala & Piacsek (1977) or in Gill (1984), however, the small differences in phase speeds among baroclinic modes yields a diminishing computational benefit for further splitting.

d. Grid Structure and Finite Differences

Figure 2 illustrates the three-dimensional grid with variables staggered in Arakawa C configuration (Arakawa & Lamb 1977). In the C configuration, mass variables such as p and ρ are defined at the full points ($\bullet$ points). The u-components ($\circ$ points), v-components ($\circ$ points), and w-components (Δ points) are defined at a half of a grid length offset from the mass points in the x-, y-, and z-directions, respectively. For the results to be reported here, a grid with $163 \times 41 \times 15$ mass points in the x-, y-, and z-directions is used with a spatial resolution $\Delta x = \Delta y = \Delta z = 2$ cm in the unstretched region. The grid can be stretched with various ratios in all three directions. In the present simulation, the grid is stretched only in the x-direction for $x > 280$ cm with a ratio equal to 1.3 : 1. This stretching allows us to simulate the slowly evolving vortices while keeping the submerged object moving downstream, and to avoid the possible adverse effect from the downstream reflecting gravity waves on the wake vortices. The spatial differences are of second order accuracy.

e. Boundary and Initial Conditions

A free-slip boundary condition is used for the horizontal velocities at the rigid bottom where the vertical velocity $w = 0$. The free-slip condition is justified since our region of interest is away from the bottom boundary. At the two walls along the direction of the moving object, a Neumann boundary condition is used. To avoid the reflection of hump waves that travel with the vehicle from the downstream wall, the stretched grid accompanying with larger K_h acts as an effective absorbing region. The initial density distribution is statically stratified with a uniform strength $N = 0.01/sec$. We have also tested a case for homogeneous fluids ($N = 0$) and produced no organized flow patterns.

f. Temporal Integration

Following Chang (1984, 1985) in his split-explicit leapfrog scheme for temporal integration, we march the barotropic and baroclinic sets of equations forward with a time interval of 0.003125 and 0.25 sec, respectively. The computation cycle starts with calculating the hydrostatic reference pressure and vertical velocity w based on the current state

of the flow. We then evaluate the transport and diffusion terms A and B in (15) and (16), and obtain $\langle A \rangle$ and $\langle B \rangle$ by vertical integration. The barotropic set set of equations is subsequently integrated 80 times with the depth average pressure gradient force updated each time step by a new h in (19), (21), and (22). The values of A' and B' remain constant during these 80 steps. The baroclinic set of equations are then integrated with the big time interval. At last we complete one computational cycle by updating all the dependent variables.

g. Tracer Injection

We also introduce a transport equation for an inert tracer with concentration Q and a source term q as follows:

$$\frac{\partial Q}{\partial t} + U\frac{\partial Q}{\partial x} + V\frac{\partial Q}{\partial y} + W\frac{\partial Q}{\partial z} = q + \frac{\partial}{\partial x}\left(K_h \frac{\partial Q}{\partial x}\right) + \frac{\partial}{\partial y}\left(K_h \frac{\partial Q}{\partial y}\right) + \frac{\partial}{\partial z}\left(K_v \frac{\partial Q}{\partial z}\right) \quad (26)$$

The purpose of this equation is to reveal the evolution of possible organized flow structures in the stratified fluid.

3. Description of the near field velocity

Modelling the near-field flow generated by a moving object is extremely difficult. The complex boundary conditions inherent in the object geometry and the high resolution required for the thin boundary layer of the object demand great computing resources. Substituting the object with a corresponding flow field within the computational domain therefore becomes a very attractive approach to circumvent these difficulties. Abernathy & Kronauer (1962) first applied this idea to simulate the instability of two parallel vortex sheets. Recently Triantafyllou & Karniadakis (1990) used this approach to simulate the vortex streets by the spectral element method. We follow the same strategy by producing a flow field that is at a finite distance from the immediate boundary of a towed sphere. This approach fits in our region of interest in which the organized flow structures develop in a region far away from the moving object.

To emulate the towed body as in several laboratory experiments (Lin & Pao 1979, Pao & Kao 1977), a spherical region with a diameter $D = 6\ cm$ is prescribed in the model to represent a towed object. Within the region, the flow velocity is artificially relaxed towards a target velocity. As shown in Figure 3, the target velocity in the x- direction (u_o) is equal to that of the prescribed moving speed of the spherical region (or the object), 4 cm/sec. The target velocity in the y- direction (v_o), flowing radially inwards to simulate a convergent flow field, is equal to a quarter of the moving speed within the spherical region. The flow at those grid points within the radius of the sphere is accelerated toward the target velocity by adding a forcing term to the horizontal equations of motion (15) and (16) as follows :

$$\frac{\partial u}{\partial t} = A - \frac{1}{\rho_o}\frac{\partial p}{\partial x} - \lambda(u - u_o) \tag{27}$$

$$\frac{\partial v}{\partial t} = B - \frac{1}{\rho_o}\frac{\partial p}{\partial y} - \lambda(v - v_o) \tag{28}$$

Here λ is the e-folding time scale for the forcing and is set to $1/sec$ in the present example. The vertical velocity w is computed by the continuity equation (5) which produces a vertical convergent flow field to simulate the vertical wake collapse phenomena.

The movement of the spherical region, with a speed of $4cm/sec$ in the downstream x-direction, is described by the trajectory of its center located right in the middle of the y-z plane. To simulate the unsteadiness of the moving body, we further introduce a random perturbation in the y-component of the center of the sphere with a maximum perturbation amplitude less than 0.2 % of the diameter of the spherical region. The introduction of the random perturbation is realistic because of the random background noise and vibrations in our environment. An amplitude of 0.001 cm is much smaller that what can be achieved in laboratories. This near field acceleration continues to be enforced as the prescribed sphere travels downstream to simulate the continuous moving of a submerged object. Furthermore, the inert tracer is released constantly from inside of

the sphere at a prescribed rate to illustrate the evolution of organized vortices in the flow field.

4. Vortex Evolution

At $t = 0$ the prescribed sphere starts moving at $x = 7$ cm. To illustrate the results, we select a horizontal plotting window that covers a region from $x = 140$ to 240 cm and $y = 16$ to 64 cm. The sphere enters from the left of the window at $t \simeq 29$ sec and exits to the right at $t \simeq 54$ sec.

The x-y plane in which the results are displayed in Figures 4 to 7 is in the middle of the channel ($z = 15$ cm) and contains the trajectory of the center of the moving sphere. Figure 4 shows the evolution of the current vectors in the middle layer at different time. At $t \leq 120$ sec, the horizontal velocity is more or less parallel to the x-direction as a result of the downstream movement of the spherical body. Later at $t = 360$ and 600 sec, the flow starts to meander, then gradually rolls up, and finally develops into organized vortices with alternating patterns as shown at later time in Figure 4. The corresponding maximum vectors for the horizontal velocity within the plotting window slowly decreases from 0.291 cm/sec at $t = 120$ sec to 0.0835 cm/sec at $t = 1800$ sec, indicating the slow rate at which the organized flow structures dissipate in the stratified fluid.

The tracer concentrations in Figure 5 illustrate the evolution of the coherent vortex patterns at the corresponding time as in Figure 4. In a very slow evolution, the patterns meander, roll up, and finally develop into vortices in the same manner as the velocity does. The evolution of the tracer pattern resembles most to what has been observed in laboratory experiments.

The density anomaly depicts similar behaviors in the development of the wake vortices as those in the velocity and tracer fields. The dash lines in Figure 6 represent negative density deviations (lighter fluid) from the initial distribution. It is apparent that the regions of lighter density are located near centers of vortices. This is consistent with the pressure balance requirement for stratified vortex motions in which lighter fluid particles with faster velocity can embed in heavier fluids (Fung 1991).

Another response of the fluid to balance the centrifugal force is the surface height perturbation. The surface signatures in Figure 7 reflect the evolution of the organized flow structure underneath once the large amplitude hump wave disperses away. The first panel in Figure 7 is the signature at $t = 120$ *sec* with a displacement ranging from -4.5 to $5 \times 10^{-5} cm$. The surface height perturbation at this time reflects only the gravity waves due to the passage of the sphere. As also illustrated at the corresponding time for the tracer, velocity, and density fields in Figures 4, 5, and 6, the surface signature reveals no organized structures within the flow field. As the initial gravity waves dissipate and the vortex patterns start evolving in those fields, however, the internal flow behavior leaves very discernible surface signatures as evident in the free surface perturbation. The corresponding displacements for the surface motion are ranging, respectively, from -2.8 to $0.6 \times 10^{-6} cm$ at $t = 360$ *sec*, to -1.1 to $0.25 \times 10^{-6} cm$ at $t = 1800$ *sec*. A perspective view for the free surface is given in Figure 8, showing the surface perturbation corresponding to the horizontal vortices. Except the one at $t = 120$ *sec* being the remnants from the passage of the sphere, the induced surface signatures respond closely to the evolution of the horizontal vortices underneath.

Even though the surface signatures shown in Figures 7 and 8 reveal the existence of the organized flow structures under the free surface, they may be affected by the depth of water and the depth at which the submerged object moves. In other words, similar internal vortex structures may produce different surface signatures when the depth of water or the depth of the moving object vary. These behavior will be discussed in a separate paper.

Figure 9 shows the velocity profile of a vertical plotting window that covers a region from $x = 140$ to 240 *cm* with the full water depth. The window is in the x-z plane located in the middle of the computation region ($y = 40$ *cm*) which contains the trajectory of the center of the moving object. Contrast to the organized patterns developing in the horizontal plane, little evidence of organized vertical structures is shown as the time evolves. This behavior is consistent with what have been observed in experiments for the horizontal vortices.

The density distribution at $t = 120$ *sec* in Figure 10 shows the density profile before the horizontal vortices develop. Layer density distributions can clearly be seen at this stage

of early wake where turbulent mixing due to the passage of the sphere is quickly suppressed by gravity. The horizontal vortices then start to evolve, and the density distribution at later time responds accordingly to balance of the centrifugal and gravitational force fields. The results for the density in the x-z plane show a different facet of the flow structure corresponding to the development of the horizontal vortices. In a deeper channel, the vertical flow structure will further reveal the coherence of the organized vortex motion. Those results will be presented in an upcoming paper.

5. A Proposal Mechanism

The resemblance of the Kármán vortex streets behind a bluff body and the horizontal vortices in stratified wakes would lead researchers to relate one to the other. To understand the generation mechanism of the horizontal vortices, one would intuitively look for a mechanism similar to that of the shedding for the Kármán vortex streets. The mechanism extended from such an intuition, however, will have to face the challenge of two fundamental questions.

First, while the velocity deficit behind a bluff body is responsible for the shedding of the Kármán vortex streets, the vortices immediately roll up behind the bluff body, become fully developed within a couple diameters behind the body, and rapidly decay as they are convected downstream. Large-scale flow structures may appear as the secondary vortex "street" in far wakes (Cimbala *et al.* 1988), however, they are not steady phenomena as compared to those vortices in the primary vortex streets or in the horizontal vortices. Even if appearing, they are only characterized by lower frequencies as the continuing development of the organized structures from the primary streets. If a similar mechanism is responsible for generating the horizontal vortices in stratified wakes, it can not explain why the horizontal vortices only appear long after the initial shedding and disturbances created by a submerged moving object have dissipated. That is a time long after the Kármán vortex streets would decay behind a bluff body. Also different from those of the secondary vortex street, the flow structures of the horizontal vortices in stratified fluids always evolve steadily from small-scale to large-scale, not only dominated by low frequencies.

Second, Kármán vortex streets exist in both homogeneous and stratified fluids. The density inhomogeneity may have influence on the detailed structures of the streets but has no bearing on their generation or existence. The horizontal vortices, on the other hand, exist only in stratified fluids. The shedding mechanism for the Kármán vortex streets cannot explain why the horizontal vortices do not exist in homogeneous fluids.

In view of the two questions just raised, the generation mechanism for the horizontal vortices must be different from that for the Kármán vortex streets. Instead of searching for the resemblance in shedding mechanism between the Kármán vortex streets and the horizontal vortices, we therefore focus on the fact that the horizontal vortices develop long after the initial induced turbulence stage is over, and that they exist only in stratified fluids. From our numerical results obtained in the present simulation, we propose a mechanism in which the density plays a crucial role in generating the horizontal vortices in stratified wakes as follows.

As the initial disturbances caused by the passage of a submerged object gradually dissipate, the buoyancy effect begins dominating the vertical motion in a stratified environment. The hydrostatic equation referenced to a fluid element with density ρ_o and pressure p_o at a depth of z_o can be written as

$$\frac{\partial}{\partial z}(p - p_o) = (\rho - \rho_o)g \tag{29}$$

where $\rho - \rho_o$ is the density anomaly which interacts with the gravity to produce an buoyancy-induced oscillation with respect to an equilibrium position z_o. The fluid element is decelerated by the gravity above the equilibrium position and accelerated by the buoyancy below the equilibrium position as described by :

$$\frac{\partial w}{\partial z} < 0 \qquad \text{for} \qquad z > z_o$$

$$\frac{\partial w}{\partial z} > 0 \qquad \text{for} \qquad z < z_o \tag{30}$$

The situation is much more complicated for vortex motions in which a centrifugal force field is present. Rotating fluids with lighter density can conceivably be embedded in an

environment of heavier density, however, the buoyancy-induced restoring force remains a dominating factor for the oscillation in stratified late wakes.

The transport equation for the z-component vorticity under the Boussinesq assumption reads

$$\frac{\partial \omega_z}{\partial t} + u\frac{\partial \omega_z}{\partial x} + v\frac{\partial \omega_z}{\partial y} + w\frac{\partial \omega_z}{\partial z} = \omega_x\frac{\partial w}{\partial x} + \omega_y\frac{\partial w}{\partial y} + \omega_z\frac{\partial w}{\partial z} + \Phi \tag{31}$$

where ω_x,ω_y, and ω_z are vorticity in the x, y, and z-direction, respectively, and Φ represents turbulence dissipation. The first three terms on the right hand side of (31) are the stretching of the three vorticity components, a vorticity forcing term in the z-direction. The last term in (31) is the result of the turbulent stresses, a diffusion term that influences the vorticity distribution.

If the vortex lines align more or less with the gravity, the vorticity in the z-direction dominates the vorticity distribution, i.e., $\omega_z >> \omega_x, \omega_y$, and the vorticity equation in the z-direction can be approximated by

$$\frac{\partial \omega_z}{\partial t} + u\frac{\partial \omega_z}{\partial x} + v\frac{\partial \omega_z}{\partial y} + w\frac{\partial \omega_z}{\partial z} \approx \omega_z\frac{\partial w}{\partial z} + \Phi \tag{32}$$

The vorticity stretching in (32), the product of the vertical velocity gradient (VVG) and the vorticity in the z-direction, becomes the main forcing term for the vorticity tendency. For a positive vorticity distribution, the vorticity increases for an upward accelerated fluid element and decreases for a downward decelerated fluid element according to (30). It is vice versa for a negative vorticity distribution. We will use our numerical results to illustrate the effect of this buoyancy-induced oscillation on the evolution of the horizontal vortices. The vorticity information will be extracted from a x-y plane in the middle of the channel where (32) is valid.

When the submerged body passes the stratified fluid as in our numerical simulation and in laboratory experiments, a three-dimensional turbulent wake column is produced. As the initial turbulence generated by the moving body is quickly damped by stratification, this wake column is under the influence of the gravity or buoyancy force in the vertical direction. The fluid is being vertically accelerated or decelerated across the wake column.

This buoyancy-induced acceleration interacts with the vorticity within the wake column in a way described by equations (30) and (32), and organizes the coherent flow patterns.

Figure 11 shows the evolution of the z-component vorticity ω_z in the horizontal plotting window ($z = 15$ cm) at different time. After the initial disturbances have decayed, a uniform vorticity distribution is created at $t = 120$ sec with positive distribution (solid lines) on one side and negative distribution (dash lines) on the other. The VVG in the corresponding region, as shown in Figure 12, interacts with the vorticity field and creates different vorticity tendencies. The vorticity is enhanced or diminished depending on whether it is in- or out-of-phase with the VVG as shown in Figure 13. The VVG at $t = 120$ sec, being positive in the vicinity of the center of the wake column, interacts with the positive vorticity (solid lines in Figure 11) on one side of the center line to produce a vorticity stretching that enhances the positive vorticity on that side. The same positive VVG also interacts with the negative vorticity (dashed lines in Figure 11) on the other side of the center line to generate a vorticity stretching that reinforces the negative vorticity distribution on the other side. In other words, the positive VVG at $t = 120$ sec reinforces both the positive and negative vorticity strength.

When the VVG becomes negative, it interacts with the wake vorticity and generates a vorticity stretching that enhances or diminishes the vorticity strength depending whether the stretching is out-of- or in-phase with the positive (or negative) vorticity.

The wake column with the z-component vorticity distribution as shown in Figure 11, though non-propagating, is transported very slowly by the induced current. As time lapses, the initial vorticity field is further modulated by the VVG, forming isolated vorticity centers. The modulation transforms the uniform vorticity distribution at $t = 120$ sec in Figure 11 to two rows of parallel and aligned isolated (relatively) vortices as shown schematically in Figure 14a. As demonstrated by von Kámán in his origin study of the Kámán vortex streets, these two rows of aligned and isolated vortices are unstable and tend to gain stability by moving into an alternative pattern (Figure 14b) as in the Kámán vortex streets. This re-alignment leads to a sinusoidal flow pattern (as observed in laboratory experiments) at $t = 360$ sec as shown in the vorticity distribution in Figure 11, in the velocity field in Figure 4, in the trace concentration in Figure 5, and in the corresponding

surface signatures in Figures 7 & 8. As the sinusoidal patterns develop, the VVG is twisted away from its original vertical direction, and re-aligns with the concentrated vorticity at $t = 360$ *sec* as shown in Figure 12. This re-aligned VVG then continues to interact with and to strengthen the local vorticity as shown in the distribution of the vorticity stretching at the same time in Figure 13. The present vorticity stretching has changed from its uniformly positive and negative distribution on both sides of the centerline at $t = 120$ *sec*, to two rows of aligned but relatively isolated distributions at $t = 360$ *sec*. This concentrated distribution has alternated positive and negative strength, and its interaction with the vorticity is becoming different than that at $t = 120$ *sec*. As shown in Figure 13 the vorticity stretching at $t = 360$ *sec* has the same positive or negative sign on both sides of the center line while the vorticity distribution at $t = 360$ *sec* is still mostly positive on one side and negative on the other, with some sinusoidal oscillations superimposed. This vorticity stretching, contrast to its earlier role at $t = 120$ *sec*, strengthens the vorticity on one side and weakens the vorticity on the other side of the center line at a certain x location, further encouraging the development of the isolated vortex pattern along the x-direction. This process is pushing the flow to evolve towards a pattern similar to that of the Kámán vortex streets.

As the concentrated vortex patterns further re-align, the VVG and the induced vorticity stretching will follow the re-alignment. The induced vorticity stretching, also alternatively in pattern as shown in Figure 13 for $t = 600$ and 840 *sec*, continues to amplify both the positive and negative vorticity on both sides of the centerline and further reinforces the development of the horizontal vortices. The corresponding flow patterns as shown in the tracer and velocity fields then reveal the patterns reminiscent of the Kámán vortex streets as observed in experiments.

In addition to the organized patterns revealed by the vorticity distribution, the magnitude of the vorticity contours also reflects the formation of the coherent structures in the stratified late wake. The magnitude of the vorticity contours ranges from -0.072 to 0.064/*sec* at 120 *sec*, -0.04 to 0.035/*sec* at 360 *sec*, -0.032 to 0.032/*sec* at 600, 840, and 1080 *sec*, -0.032 to 0.028/*sec* at 1320 and 1560 *sec*. and -0.036 to 0.028/*sec* at 1800 *sec*. The change of magnitude between $t = 120$ and $t = 360$ *sec* are quite distinct and reflects

the wake structure change before and after the onset of the vortex development. By the time the sinusoidal patterns begin to form, the vorticity strength show little change as an indication of the existence and persistence of the horizontal vortices within the flow field.

The proposed mechanism for the evolution of the horizontal vortices is based on the vorticity stretching in the vertical direction. This stretching is a result of the interaction of local vorticity produced by the wake remnants of a submerged moving body, and the vertical velocity gradient resulting from the buoyance effect of the density stratification. The interaction becomes the driving force that generates and reinforces the evolution of the alternating and concentrated vortex patterns as observed in laboratory experiments. This mechanism explains the delay appearance of the horizontal vortices in late wakes, and their vital dependency on stratified fluids.

6. Summary

The organized flow structure generated by a submerged object moving in a stratified fluid is simulated by a three-dimensional time-dependent numerical model. The flow is assumed to be incompressible and hydrostatic with the Boussinesq approximation for a weakly stratified fluid. The horizontal turbulent mixing is modeled by the Smagorinsky formula to admit the rate of deformation, whereas the vertical mixing is based on a Richardson number closure to account for the density and shear effects in stratified fluids. Preliminary results for the velocity, density, and tracer fields consistently show the existence and evolution of such organized flow structures within a stratified flow field. The surface signatures consequently reveal the development of such vortex structure underneath.

A mechanism based on the interaction of the wake vorticity and the buoyancy effect in a stratified fluid is proposed for the generation and growth of the horizontal vortices in stratified fluids. The resultant vorticity stretching is the driving force for the evolution of the organized patterns, from meandering to the fully rolled-up structures reminiscent of the Kámán vortex streets. A test case for homogeneous fluids showed no development of horizontal vortices. This mechanism explains the delayed appearance of the horizontal vortices and their vital dependency on stratified fluids. Furthermore, our results suggest

that simple two-dimensional models cannot adequately describe the motion and characteristics of the horizontal vortices. Only models in which the vertical stratification is properly represented are suitable for simulating these vortices.

In this paper only one case of a series of numerical experiments has been presented and discussed. Various sensitivity tests can be conducted to isolate effects of different parameters such as the depth of the fluid, the strength of the stratification, the size, the shape, the speed and the depth of the moving object, etc. These and other results will be presented in an upcoming paper.

References

Abernalthy, F. H. & Kronauer, R. E., (1962) " The Formation of Vortex Streets," *Journal of Fluid Mechanics*, Vol. 13, p.1.

Arakawa, A., & Lamb, V. R. (1977) "Computational design of the basic dynamical process of the UCLA general circulation model," *Methods in Computational Physics*, Vol. 17, Academics Press, p. 173.

Barnett, K. M., (1972) "A Wind Trunnel Experiment Concerning Atmospheric Vortex Street," *Boundary Layer Meteorology*, Vol 2, p. 427.

Chang, S. W. (1984) "A Split-Explicit Integration Method for Ocean Dynamics Models," *Papers in Meteorology Research*, Vol 7, p. 1.

Chang, S. W. (1985) "Deep Ocean Response to Hurricanes as Revealed by an Ocean Model with Free Surface — Part I. Axisymmetric Case," *Journal of Physical Oceanography*, Vol 15, p. 1847.

Chopra, K. P., (1973) "Atmospheric and Oceanic Flow Problem Introduced by Islands," *Advances in Geophysics*, Vol 16, p. 297.

Chopra, K. P. & Hubert, L. F., (1965) "Meso-Scale Eddies in Wake of Islands," *Journal of Atmospheric Sciences*, Vol 22, p. 652.

Cimbala, J. M., Bagib, H. M., & Roshko, A., (1988) "Large Structure in the Far Wakes of Two-Dimensional Bluff Bodies," *Journal of Fluid Mechanics*, Vol 190, p. 265.

Davis, R. E. & Acrivos, A., (1967) "Solitary Internal Waves in Deep Water," *Journal of Fluid Mechanics*, Vol 29, p. 593.

Fung, Y. T., (1983) "Stability Characteristics for Flows of the Vortex-Sheet Type," *Journal of Fluid Mechanics*, Vol 135, p. 201.

Fung, Y. T., (1986) "Richardson Criteria for Stratified Vortex Motions under Gravity," *The Physics of Fluids*, Vol 29, p. 368.

Fung, Y. T., (1991) "Nonaxisymmetric Waves of a Stratified Vertical Vortex," *Journal of Applied Mechanics*, to be published.

Fung, Y. T. & Kurzweg, U. H., (1975) "Stability of Swirling Flows with Radius- Dependent Density," *Journal of Fluid Mechanics*, Vol 72, p. 243.

Fung, Y. T., (1991) "Non-axisymmetric Waves of a Stratified Vertical Vortex," *Journal of Applied Mechanics*, to be published.

Howard, L. N., (1961) "Note on a Paper of John Miles," *Journal of Fluid Mechanics*, Vol 10, p. 509.

Kao, T. W. & Pao, H. P., (1979) " Wake Collapse in the Thermocline and Internal Solitary Waves," *Journal of Fluid Mechanics*, Vol 97, p. 115.

Karniadikis, G. E. & Triantafyllou, G. S. (1989) "Frequency Selection and asymptotic States in Laminar Wakes," *Journal of Fluid Mechanics*, Vol 199, p. 441.

Lin, J. T. & Pao Y. H., (1979) " Wakes in Stratified Fluids," *Annual Review of Fluid Mechanics*, Vol 11, p. 317.

Lyons, W. & Fujita, T., (1968) "Mesoscale Motions in Oceanic Stratus as Revealed by Satellite Data," *Monthly Weather Review*, Vol 96, p. 304.

Miles, J. W., (1961) "On the Stability of Heterogenous Shear Flows," *Journal of Fluid Mechanics*, Vol 10, p. 496.

Pao, H. P. & Kao, T. W., (1976) " On Vortex Trails over Ocean Islands," *Atmospheric Science (Meteorological Society of the Republic of China)*, Vol. 3, p. 28.

Pao, H. P. & Kao, T. W. (1977) "Vortex structure in the Wake of a Sphere," *The Physics of Fluids*, Vol 20, p. 187.

Thomson, R. E., Gower, J. F. R., & Bowker, N. W. (1977) "Vortex Streets in the Wake of Aleutian Islands," *Monthly Weather Review*, Vol 105, p. 873.

Triantafyllou, G. S. & Karniadikis, G. E. (1990) "Computational Reducibility of Unsteady Viscous Flows," *The Physics of Fluids*, Vol 2, p. 653.

Wu, J., (1969) "Mixed Region Collapse with Internal Wave Generation in A Density-Stratified Medium," *Journal of Fluid Mechanics*, Vol 35, p. 531.

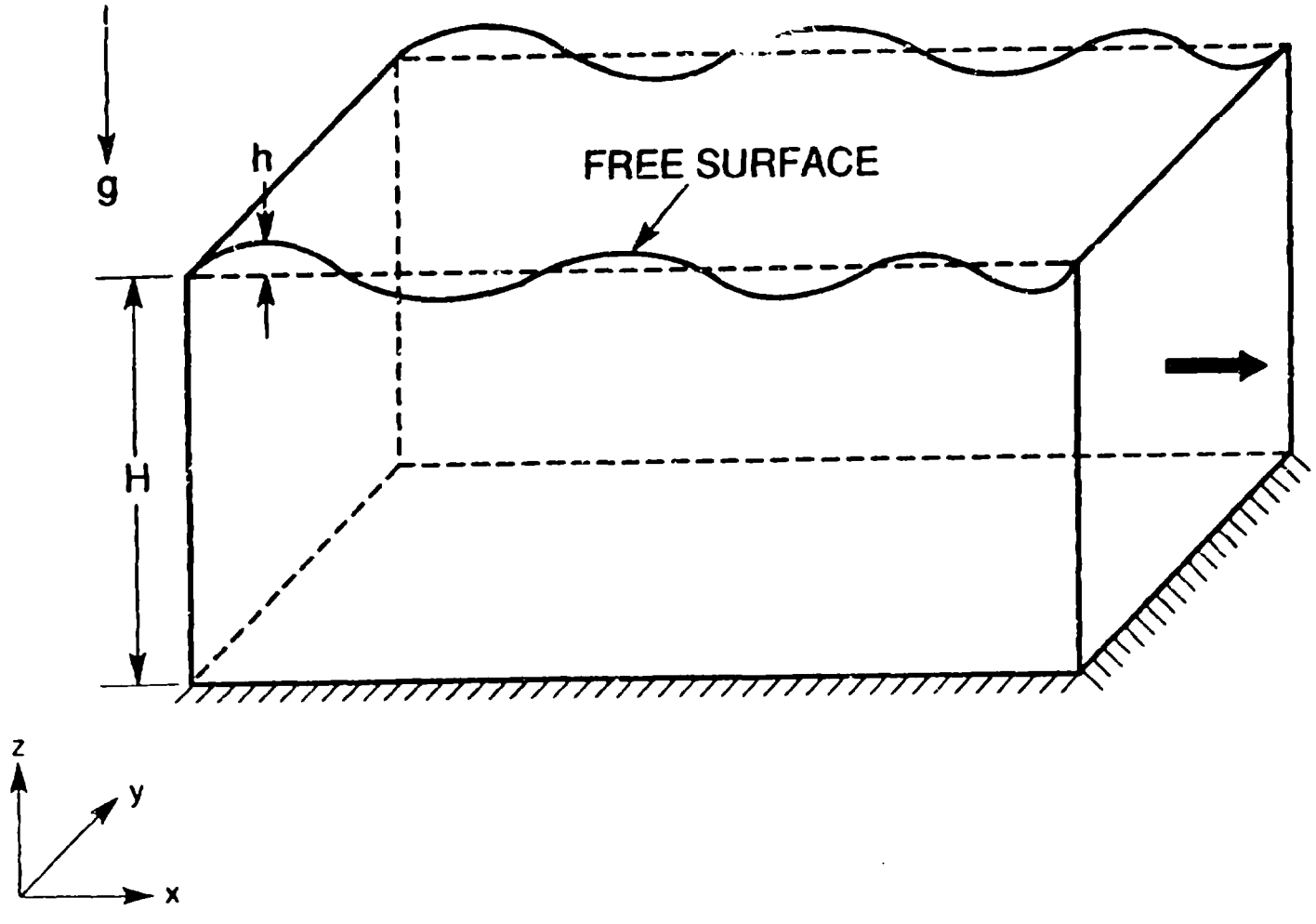

Figure 1. Physical domain of the 3D numerical model with a free surface.

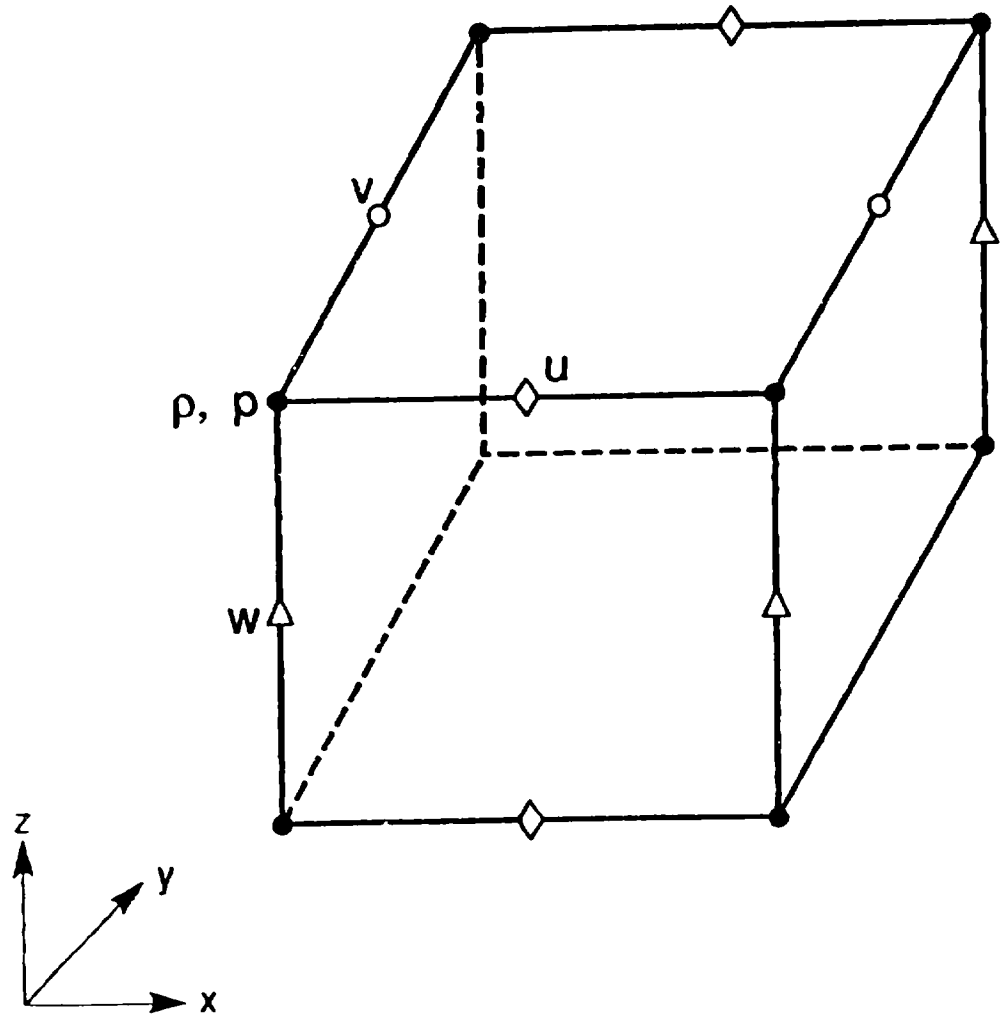

Figure 2. Staggered grid with velocity components defined at half of a grid length from mass points.

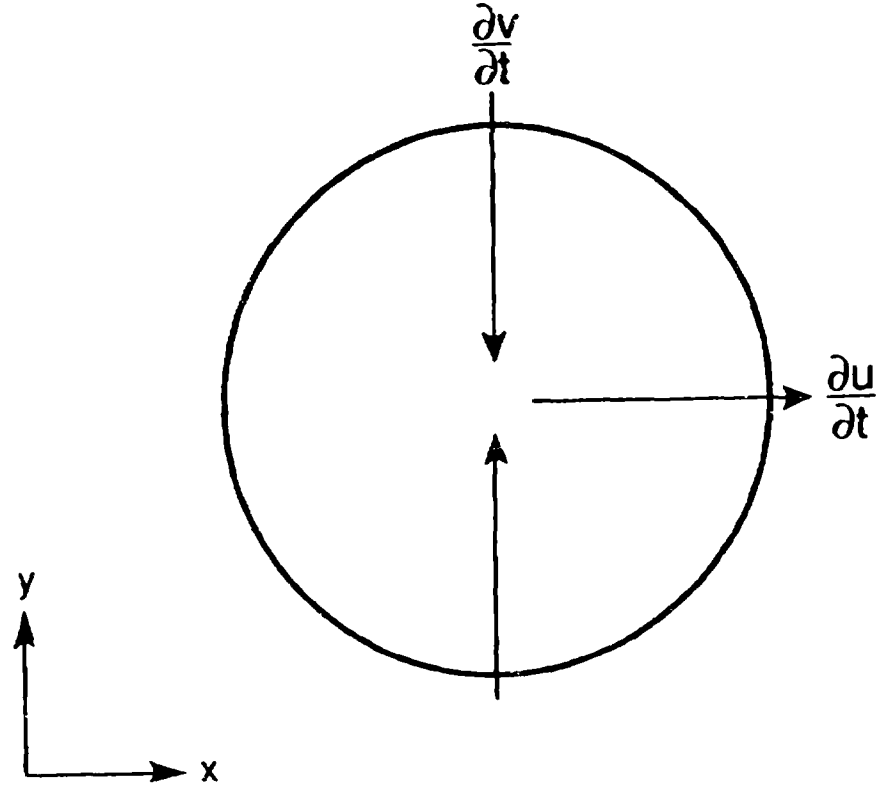

Figure 3. Prescribed acceleration for the flow field within the spherical region.

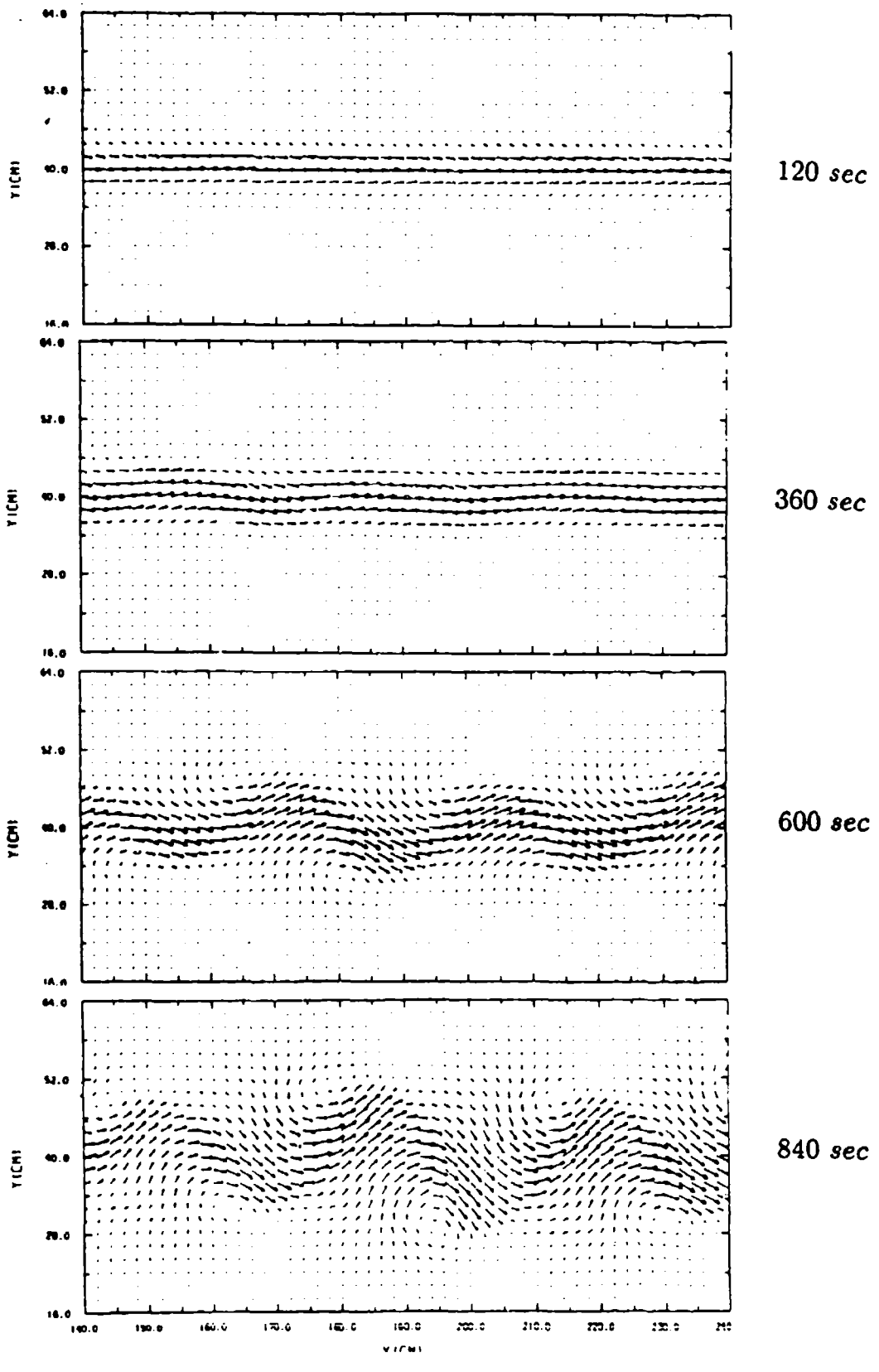

Figure 4. Velocity vectors in a horizontal plotting window (x-y plane at $z = 15\ cm$) in the middle of the channel.

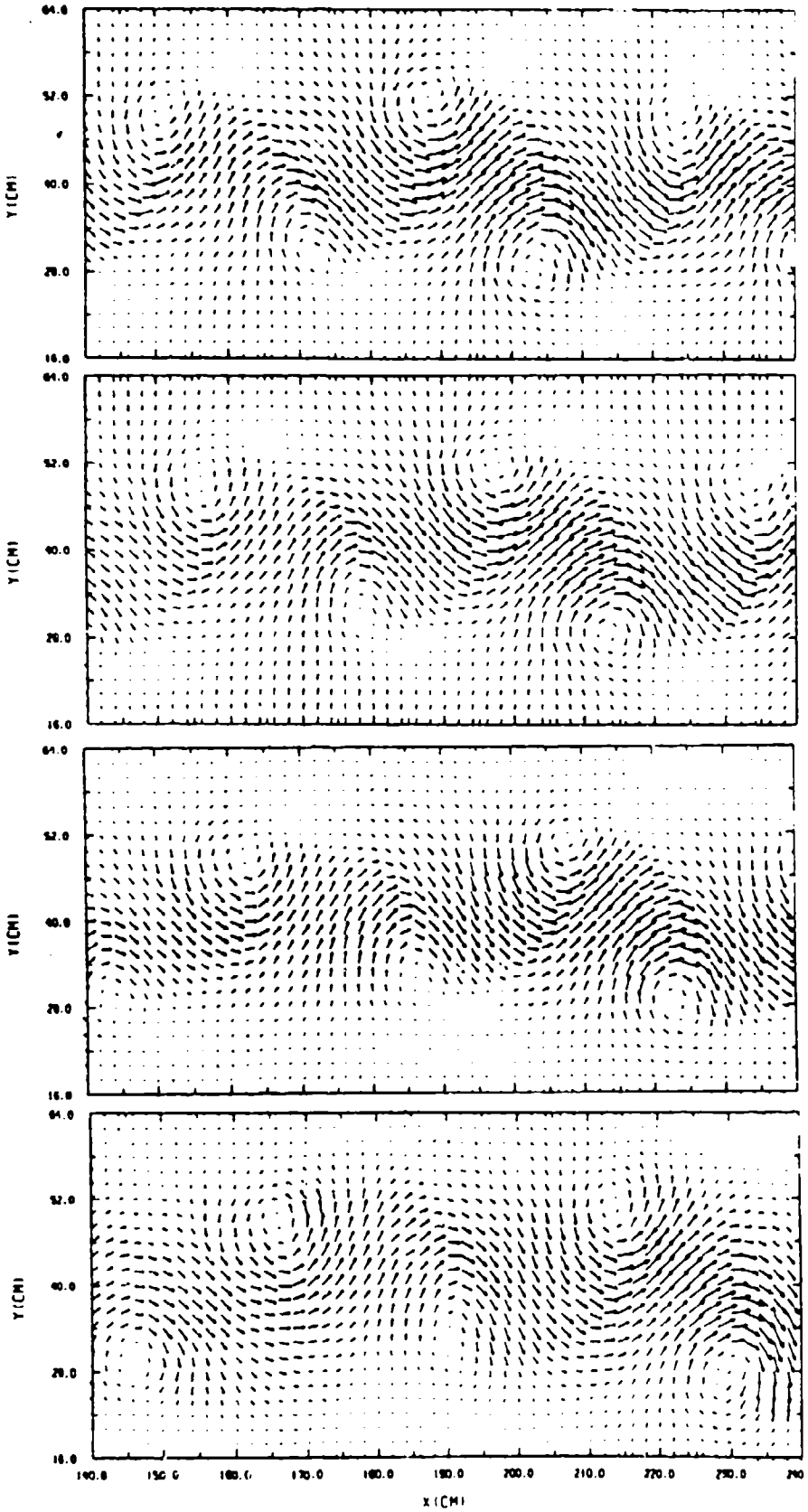

Figure 4. Continued.

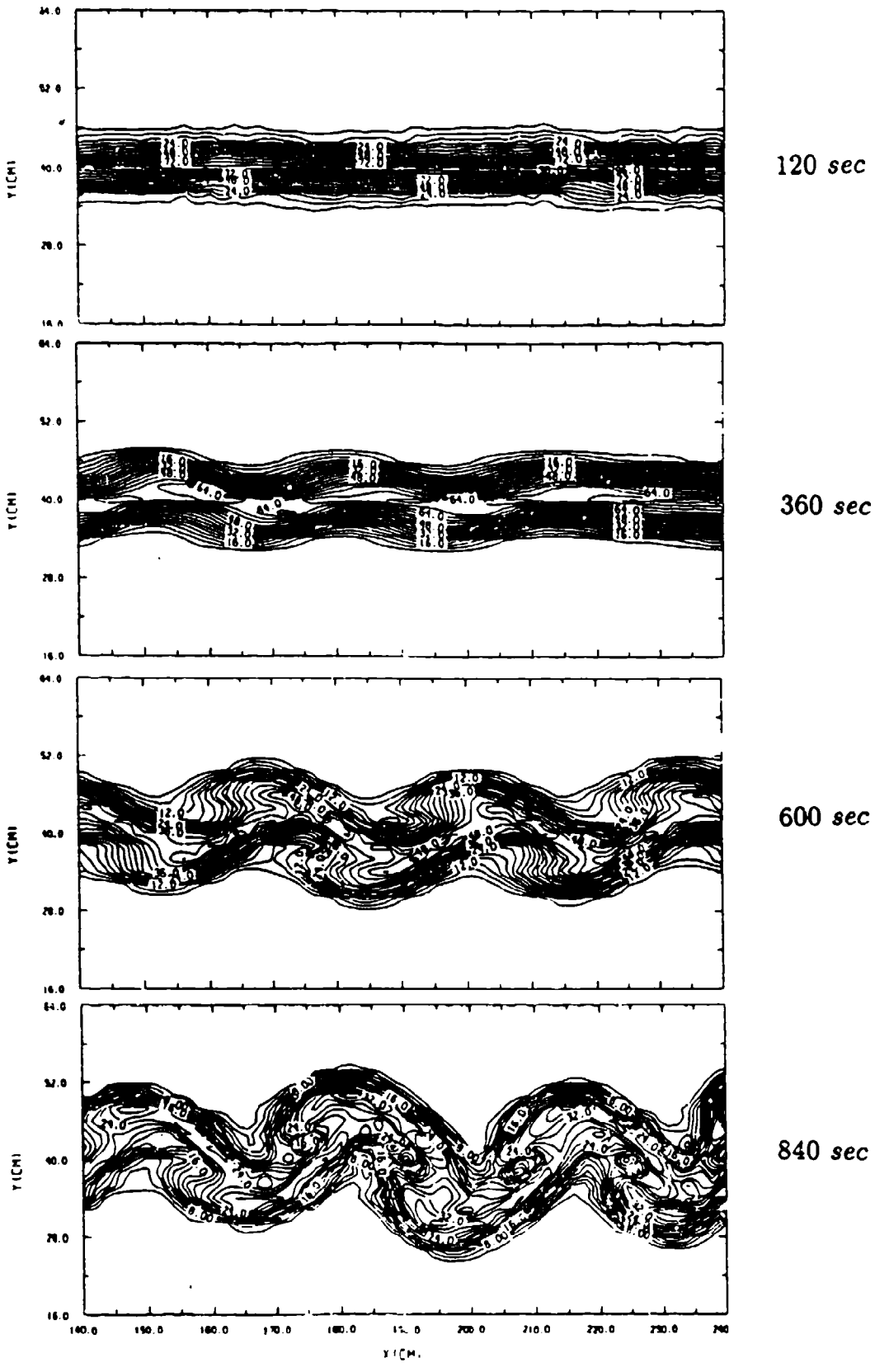

Figure 5. Tracer concentration in a horizontal plotting window (x-y plane at $z = 15$ cm) in the middle of the channel.

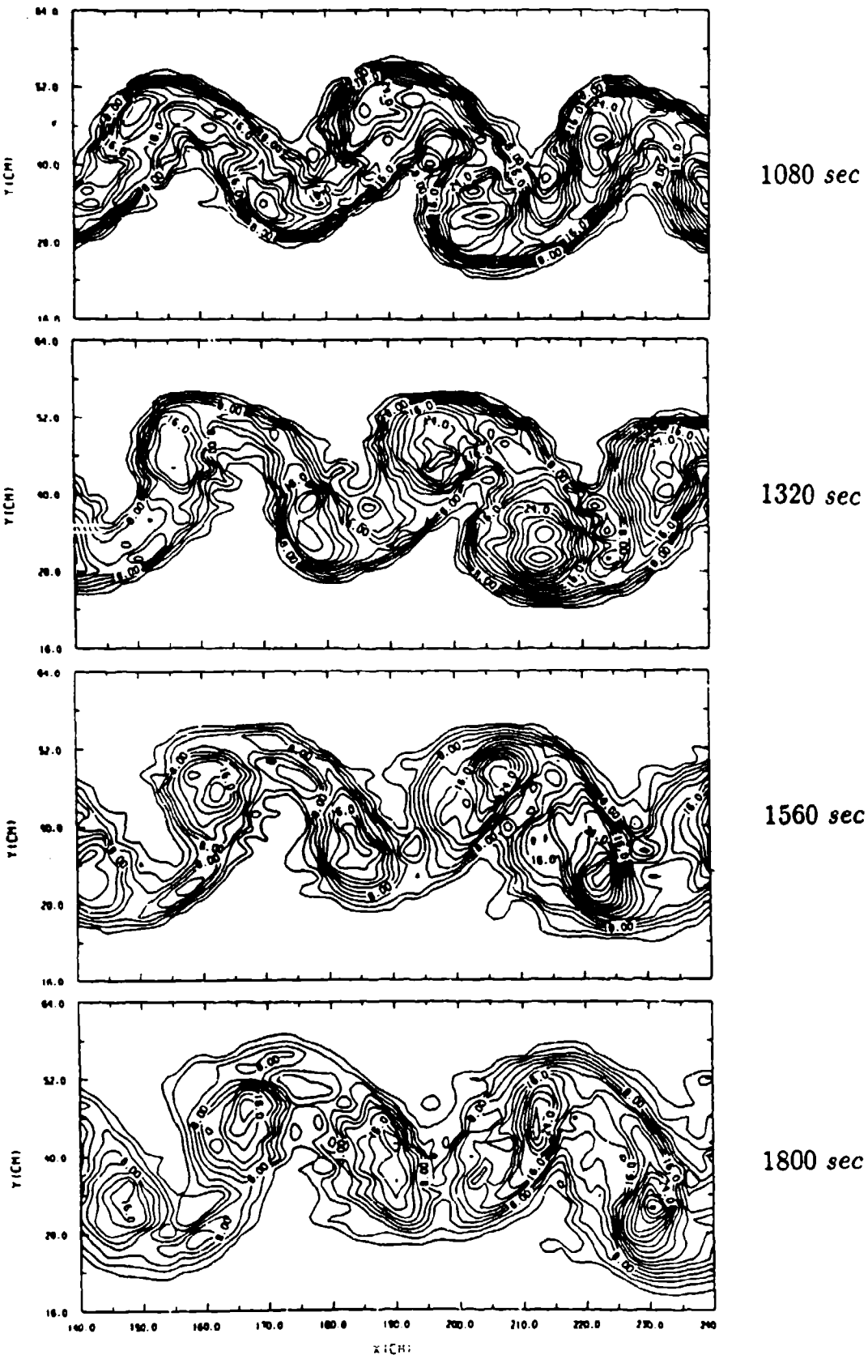

Figure 5. Continued.

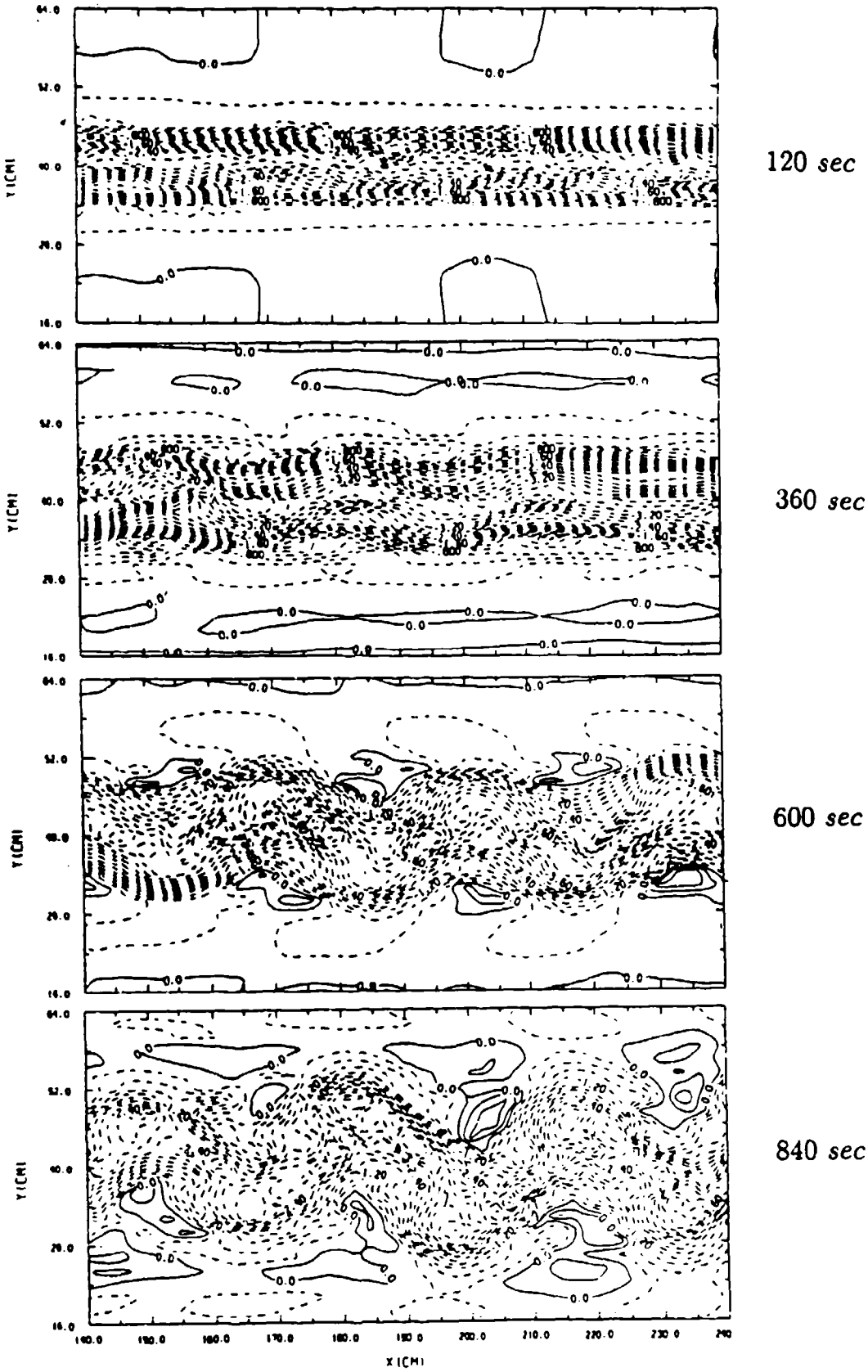

Figure 6. Density anomaly in a horizontal plotting window (x-y plane at z = 15 cm) in the middle of the channel.

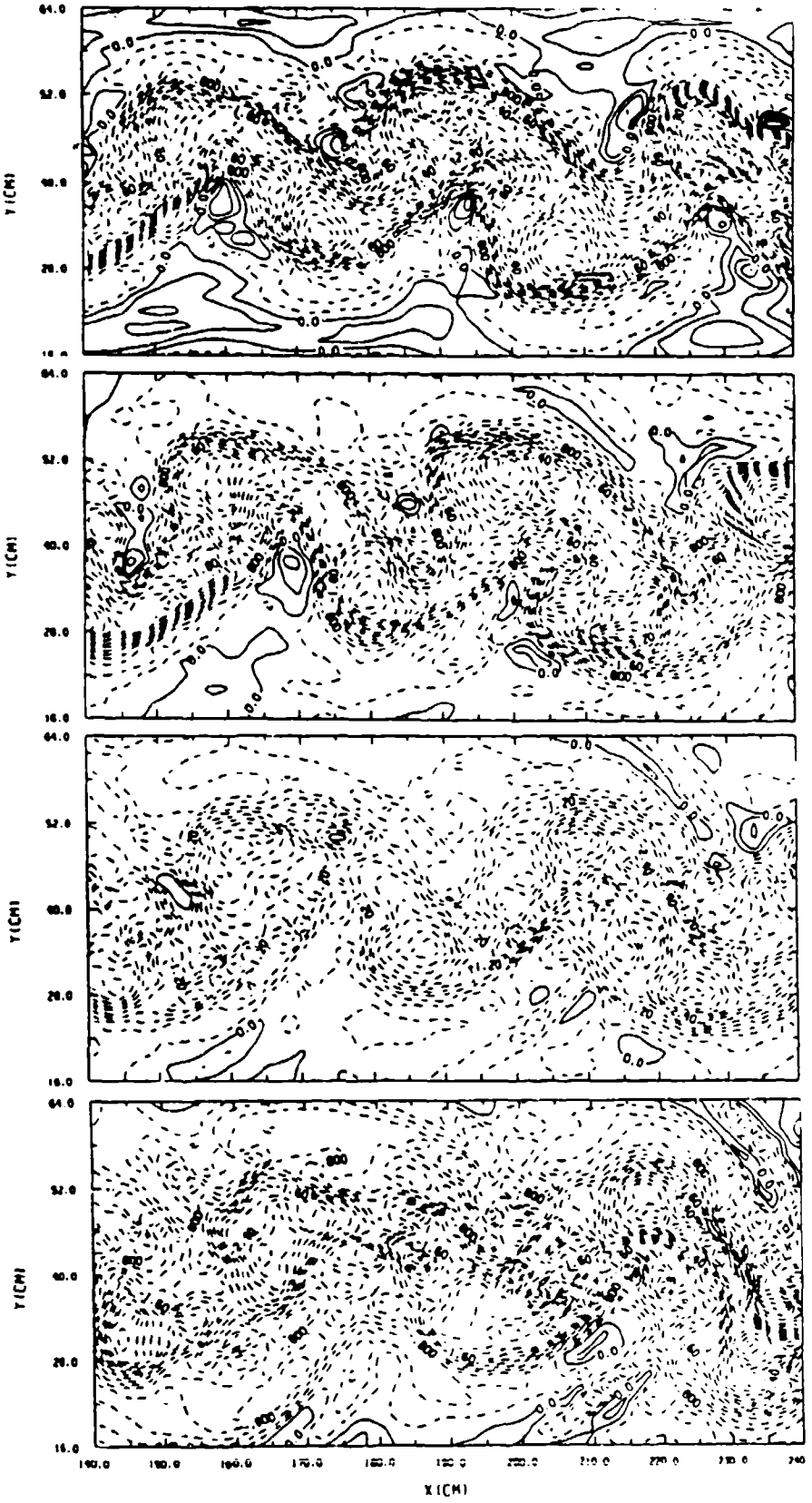

Figure 6. Continued.

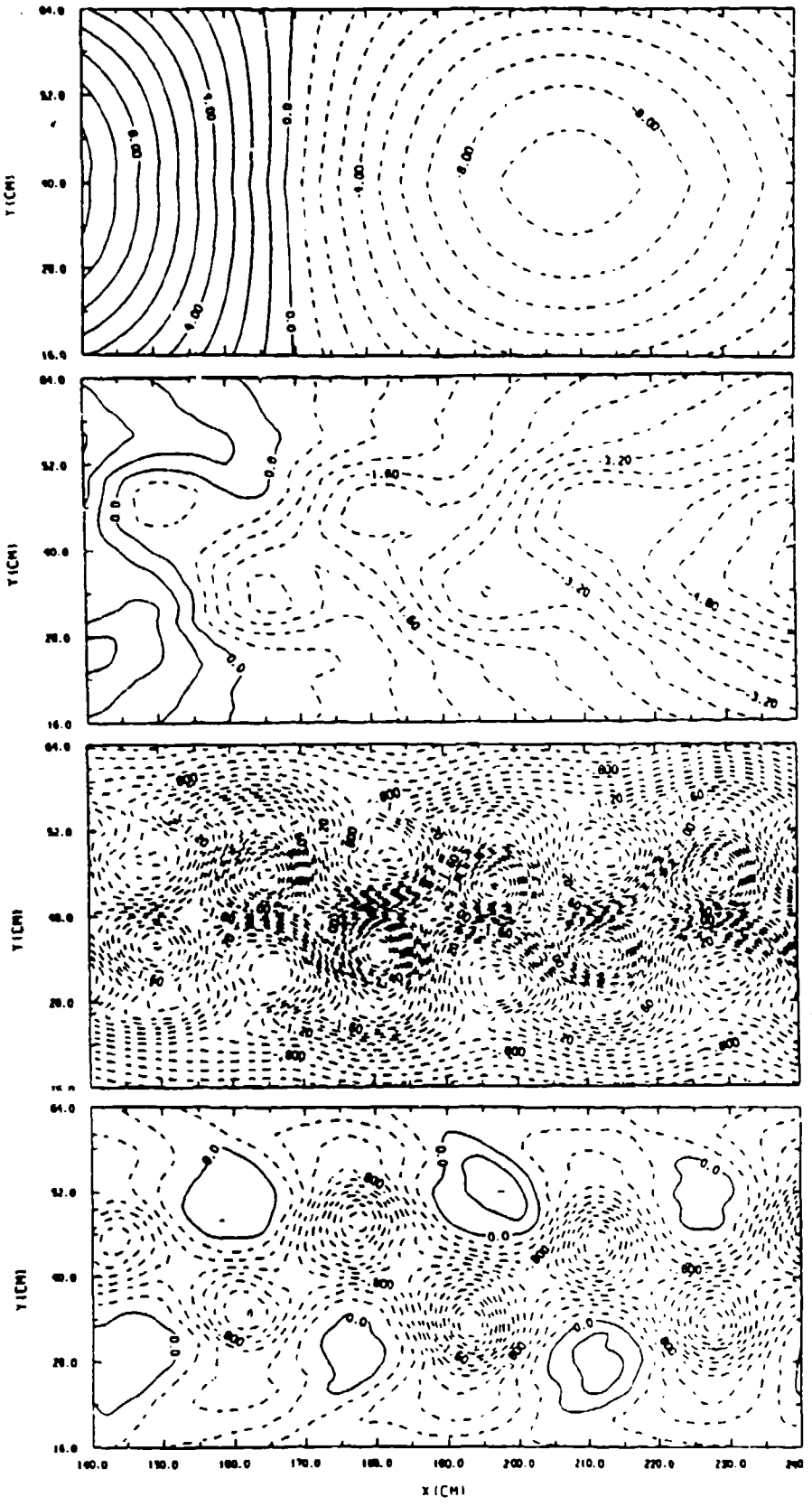

Figure 7. Free surface contours in a horizontal plotting window.

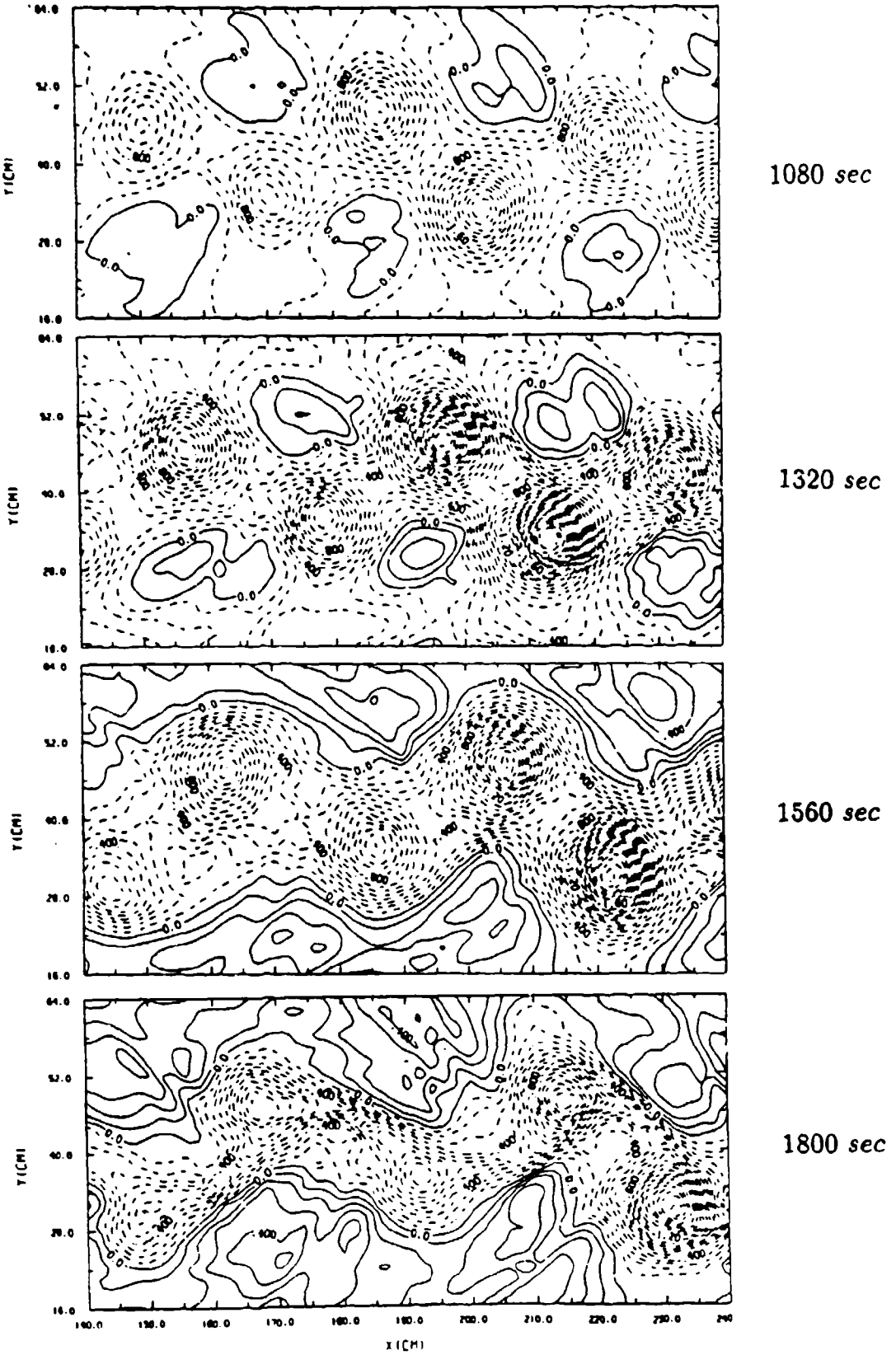

Figure 7. Continued.

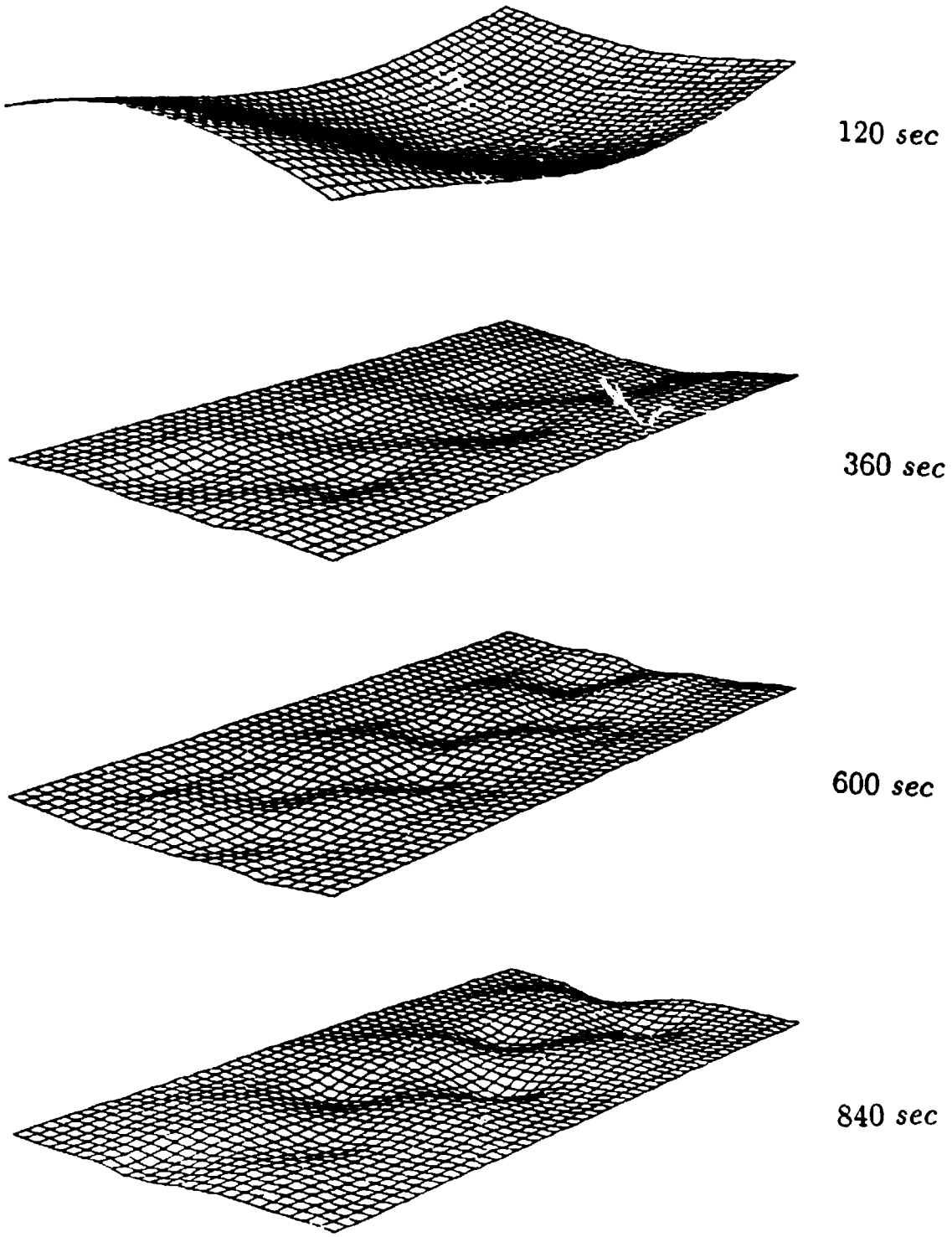

Figure 8. Perspective view for the free surface signatures in Figure 7.

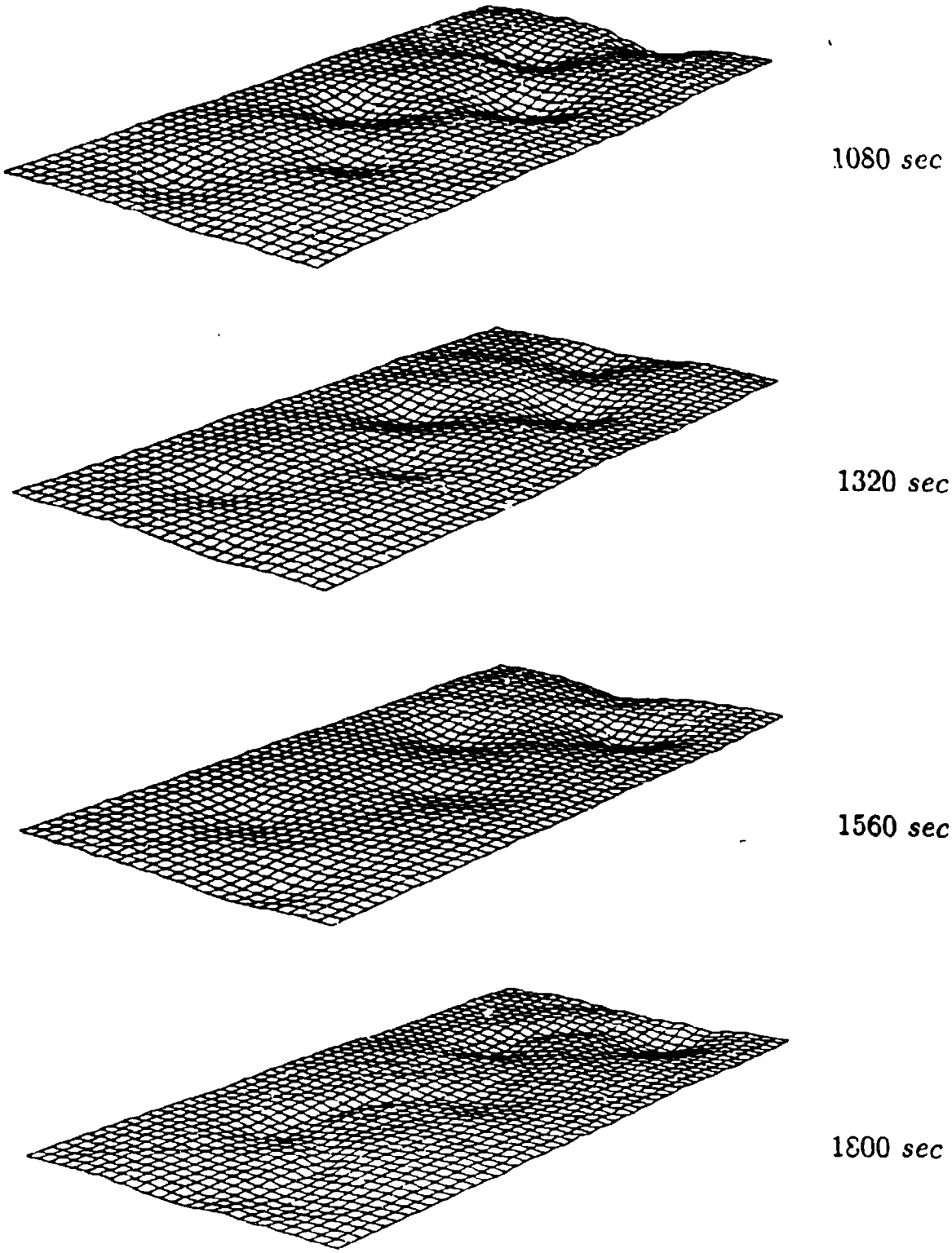

Figure 8. Continued.

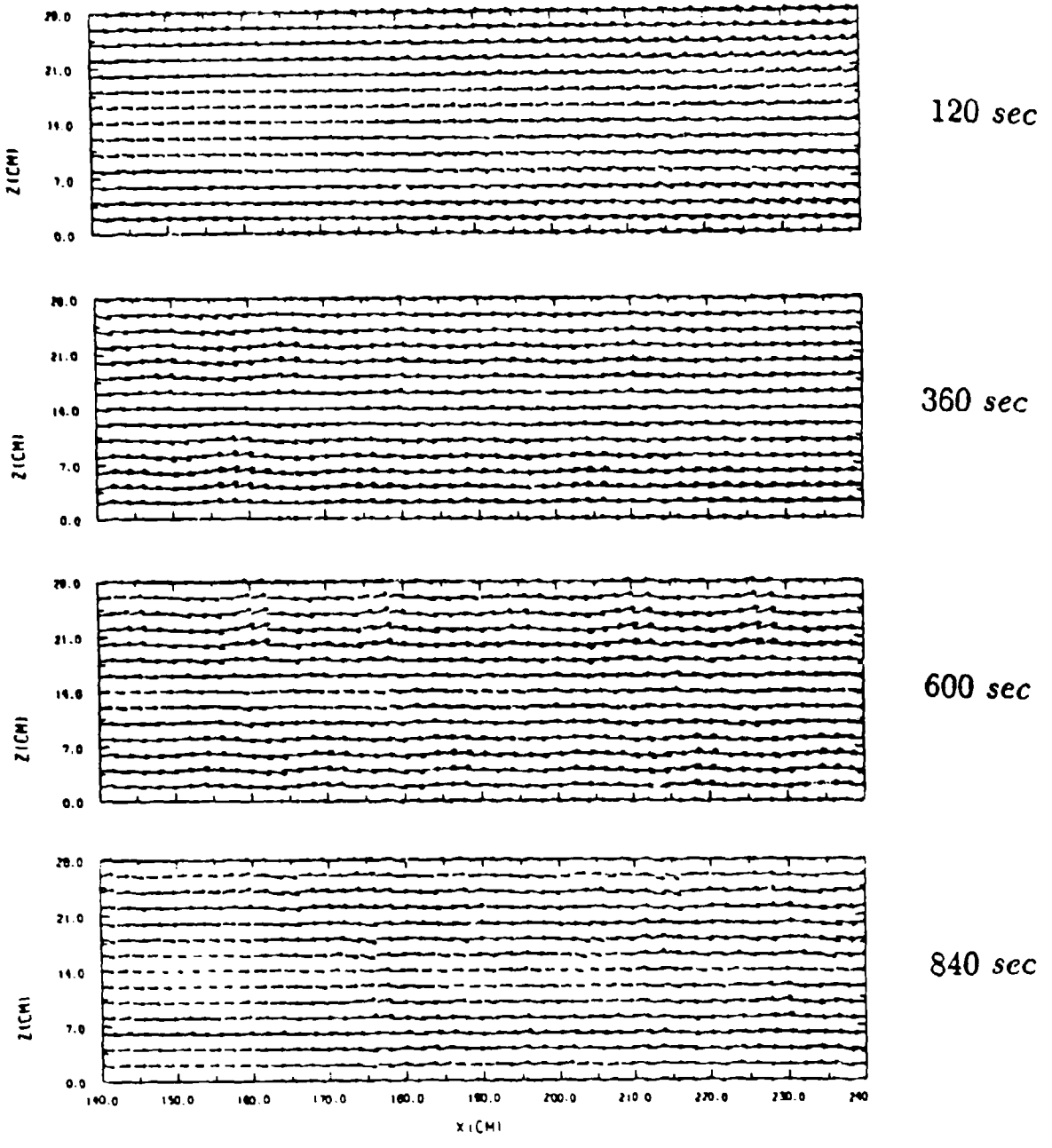

Figure 9. Velocity vector in a vertical plotting window (x-z plane at $y = 40$ cm) in the middle of the channel..

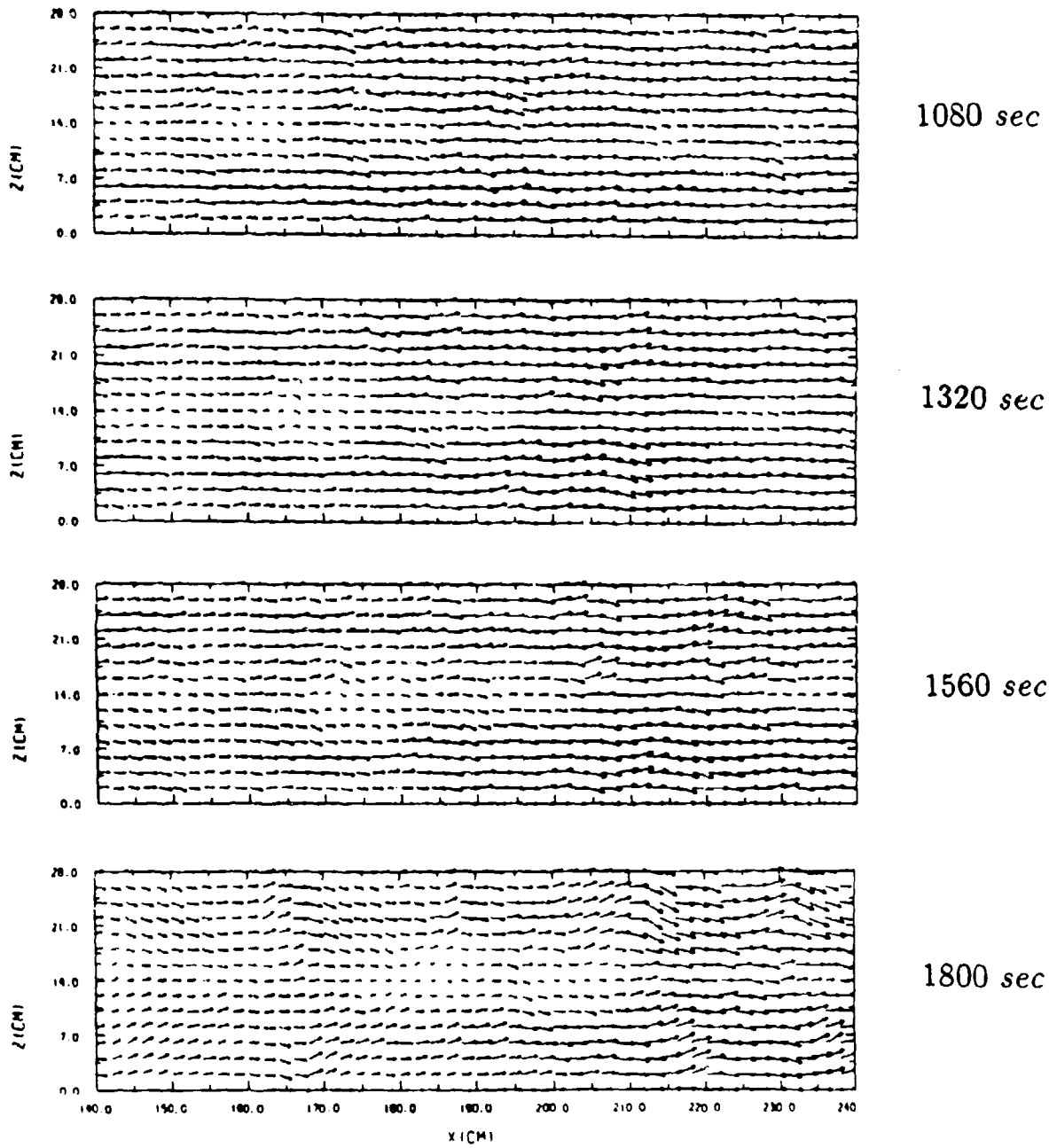

Figure 9. Continued.

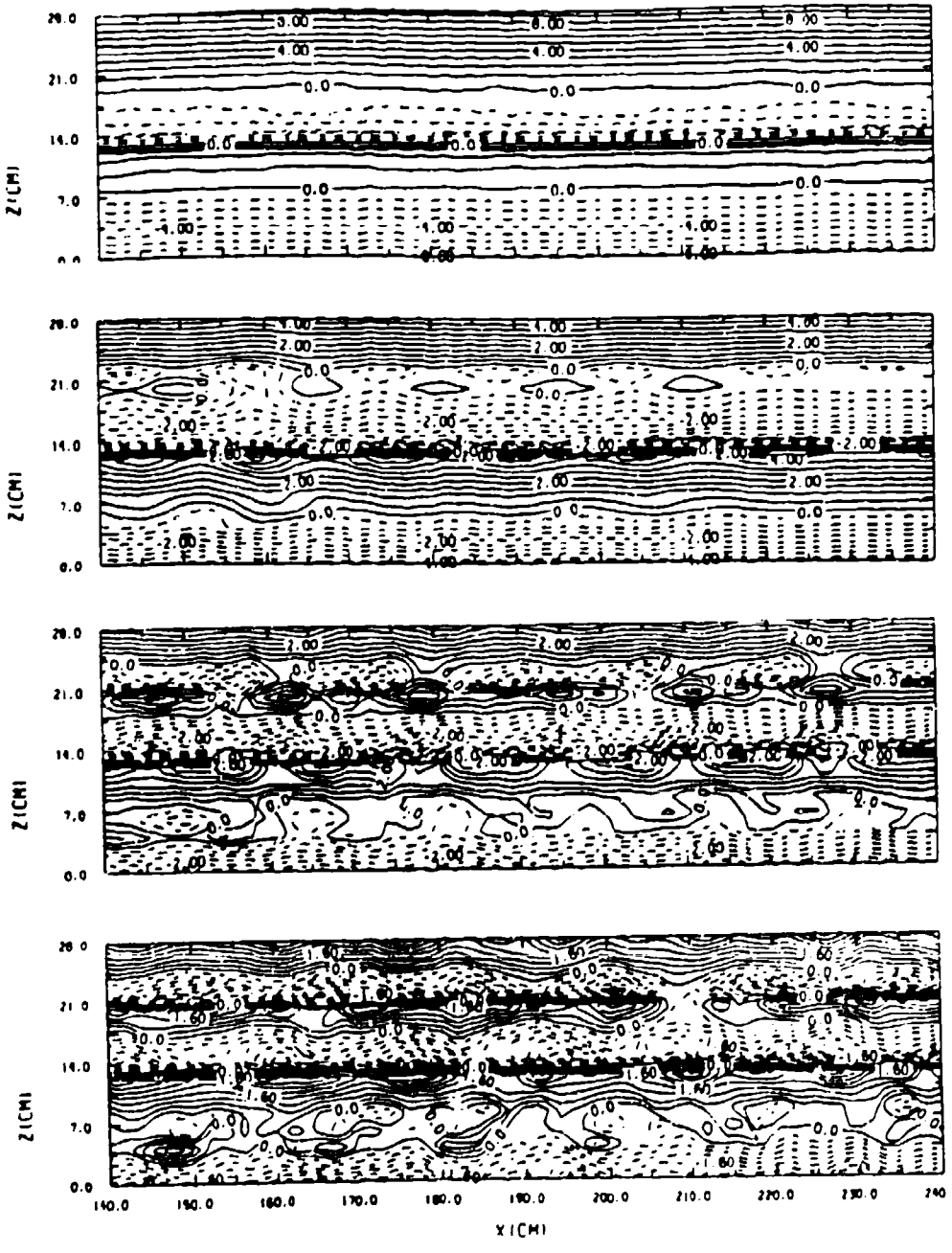

Figure 10. Density anomaly in a vertical plotting window (x-z plane at $y = 40\ cm$) in the middle of the channel..

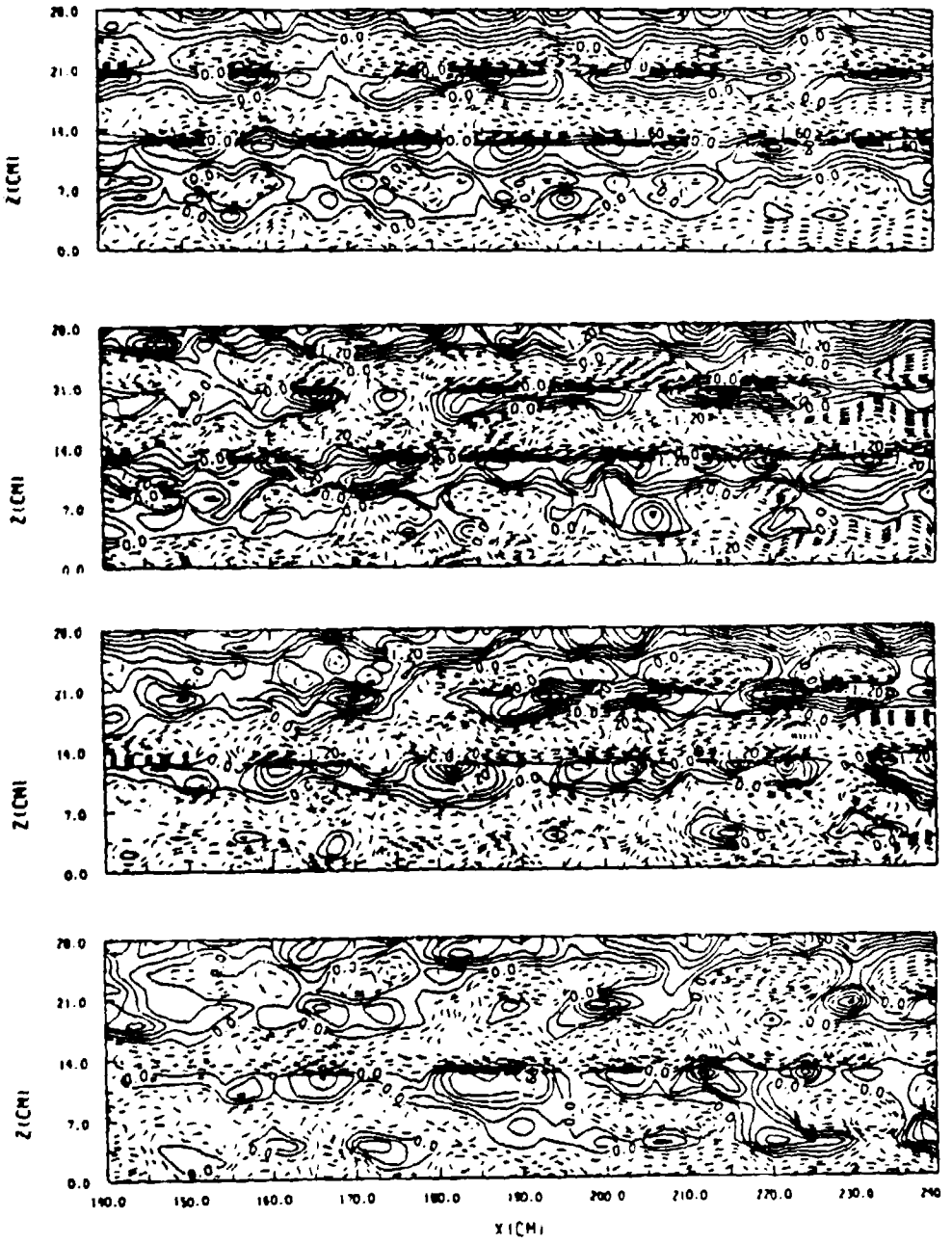

Figure 10. Continued.

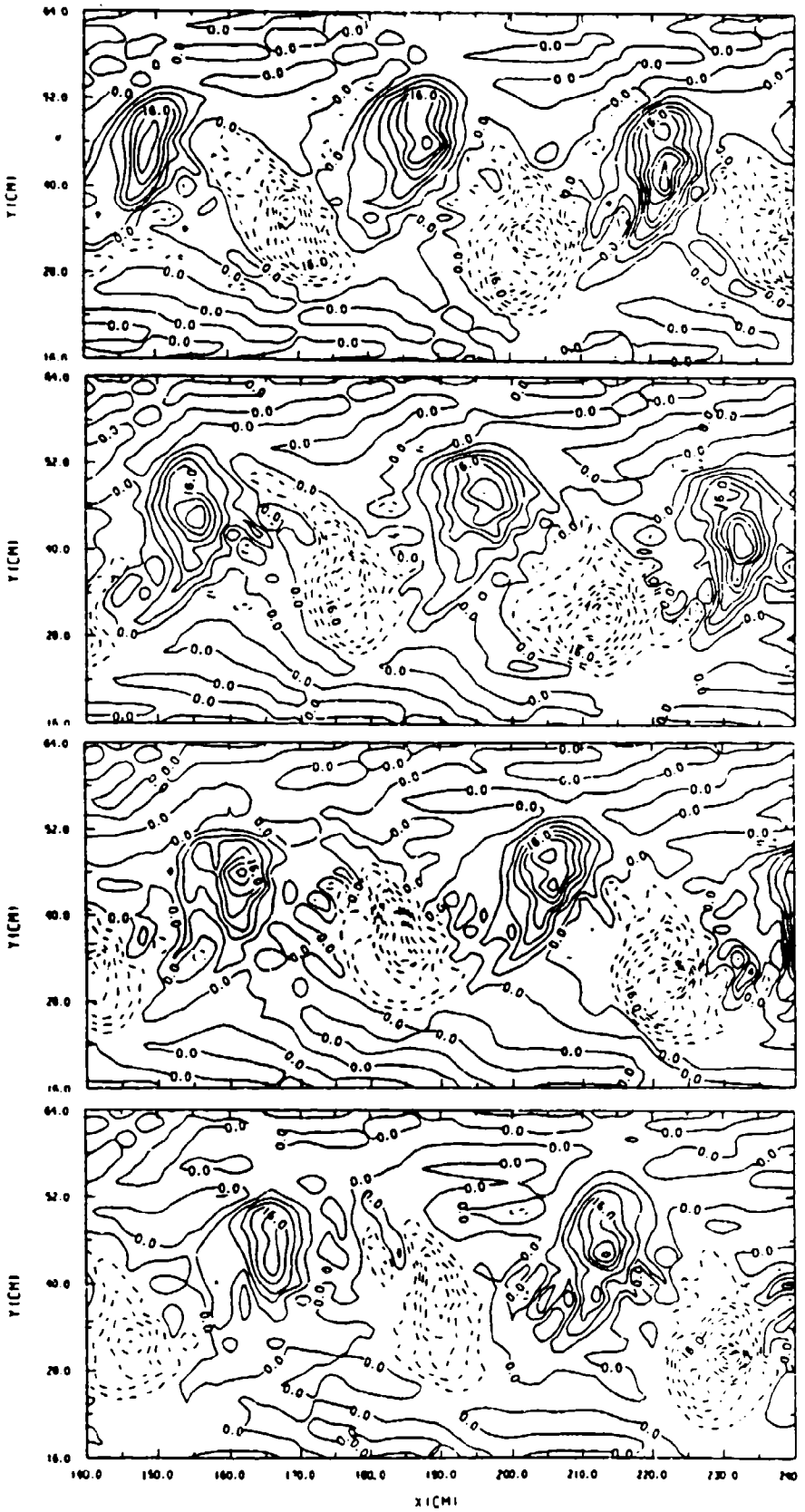

Figure 11. Continued.

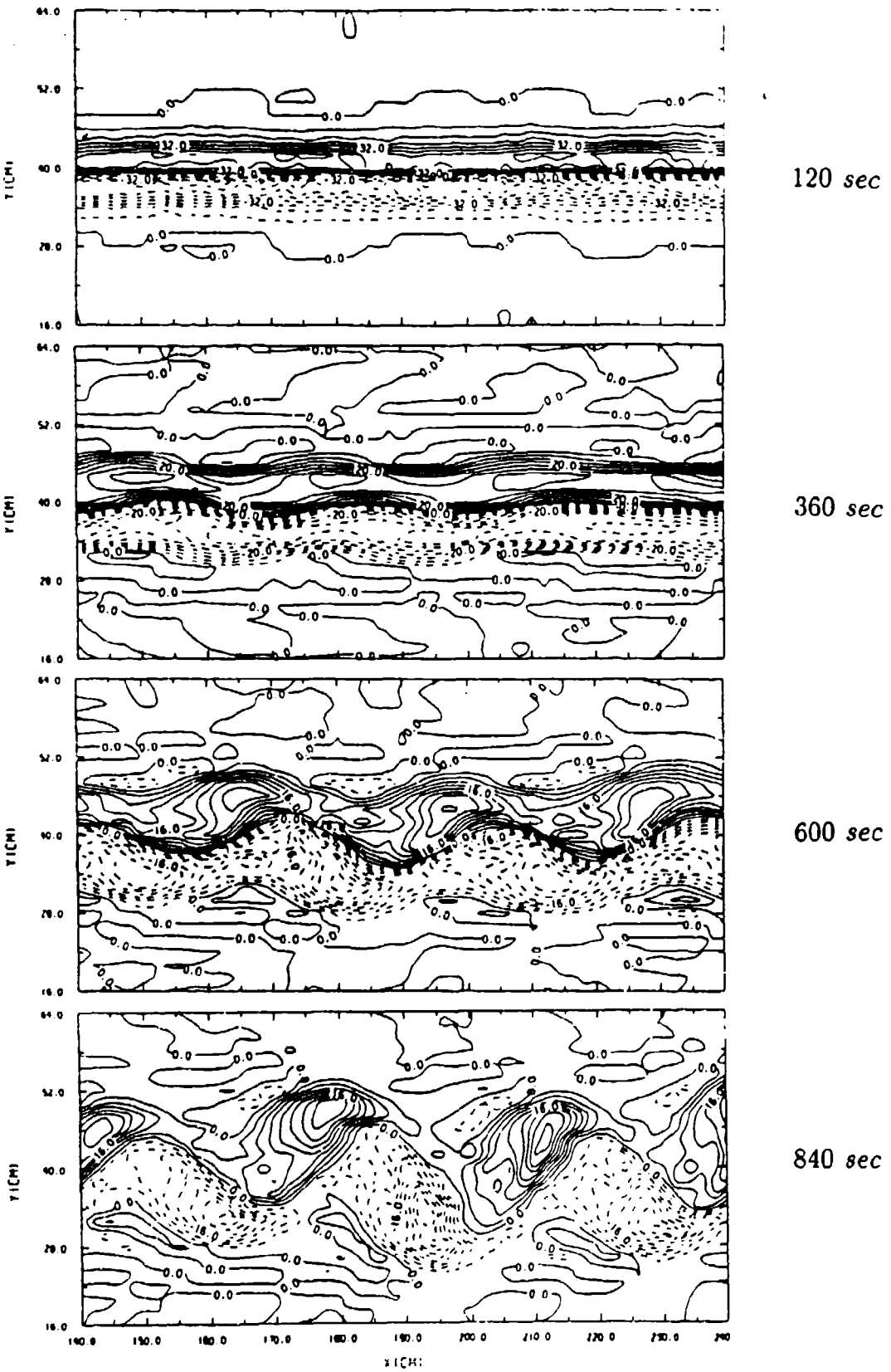

Figure 11. Z-component vorticity (ω_z) in a horizontal plotting window (x-y plane at $z = 15$ cm) in the middle of the channel.

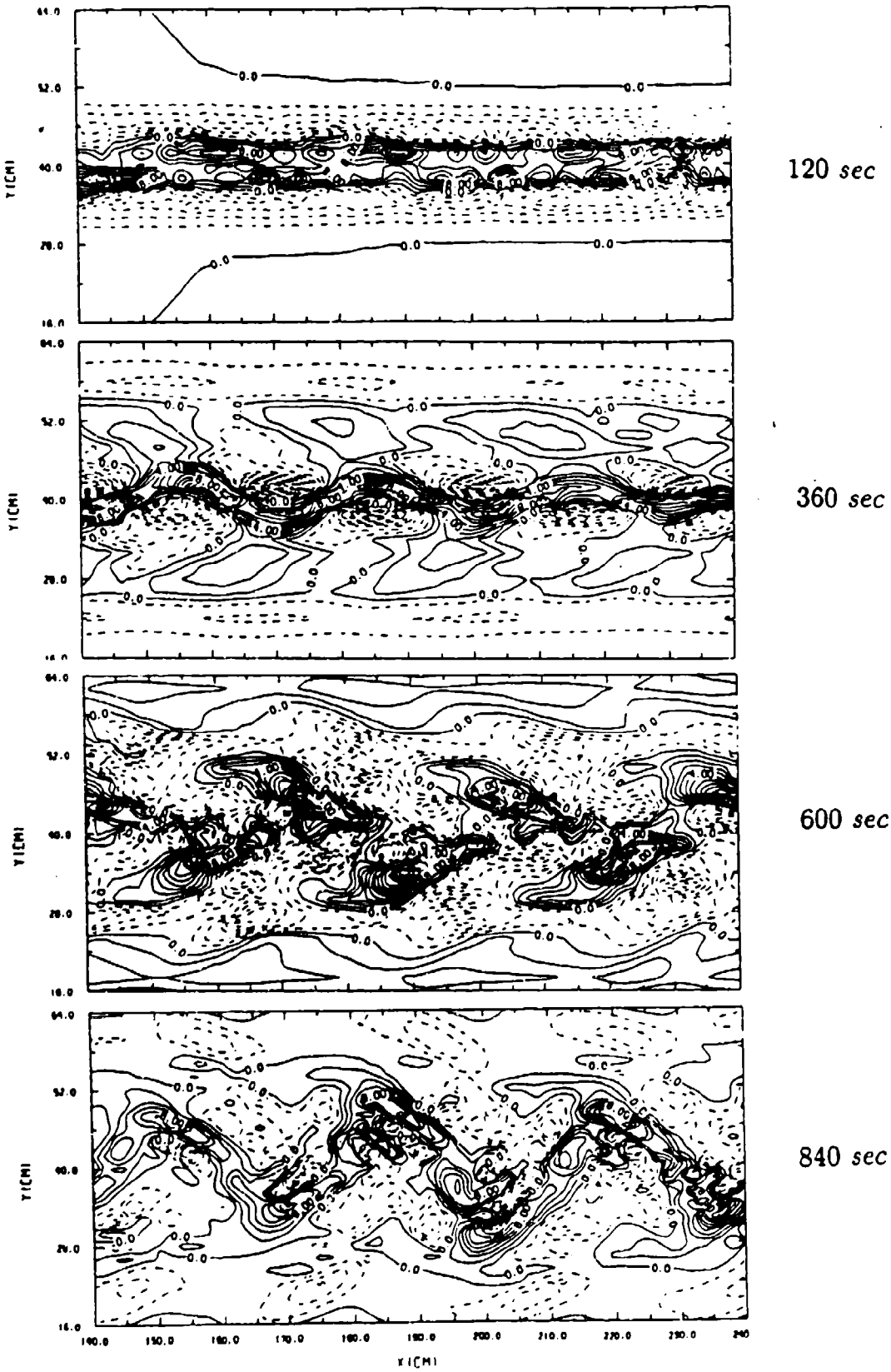

Figure 12. Vertical velocity gradient in a horizontal plotting window (x-y plane at z = 15 cm) in the middle of the channel.

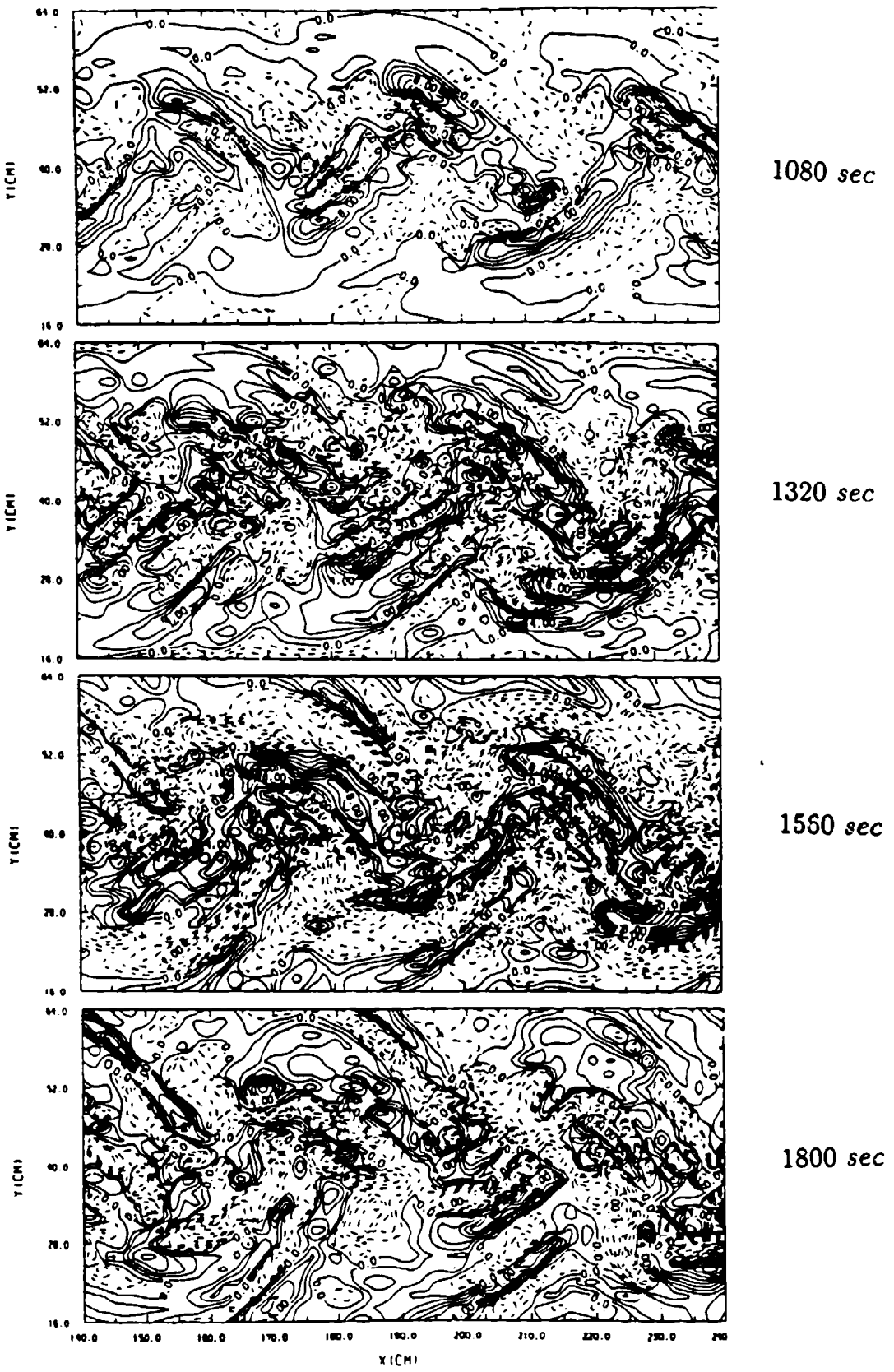

Figure 12. Continued.

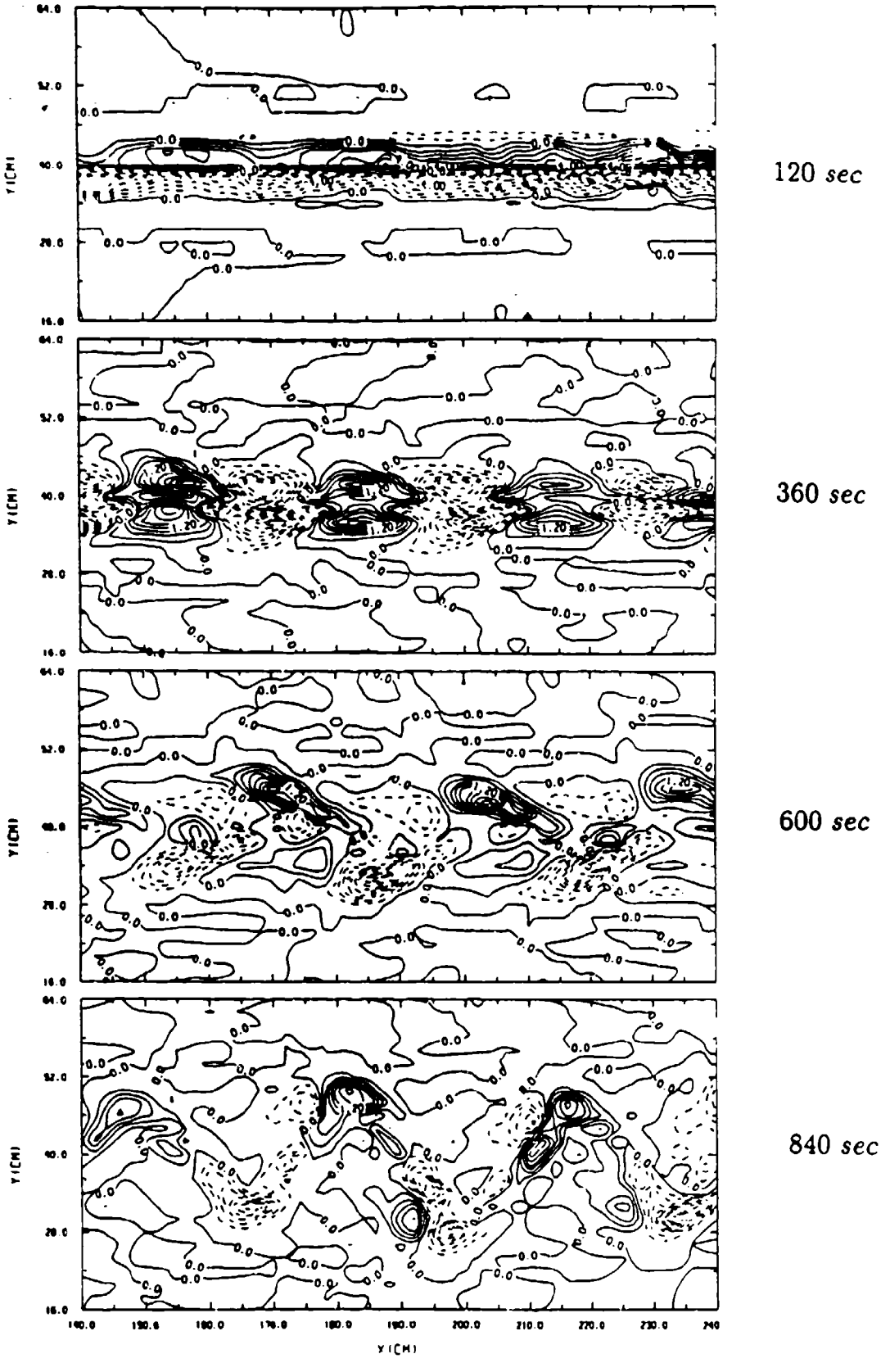

Figure 13. Z-component vorticity stretching ($\omega_z \frac{\partial w}{\partial z}$) in a horizontal plotting window (x-y plane at $z = 15$ cm) in the middle of the channel.

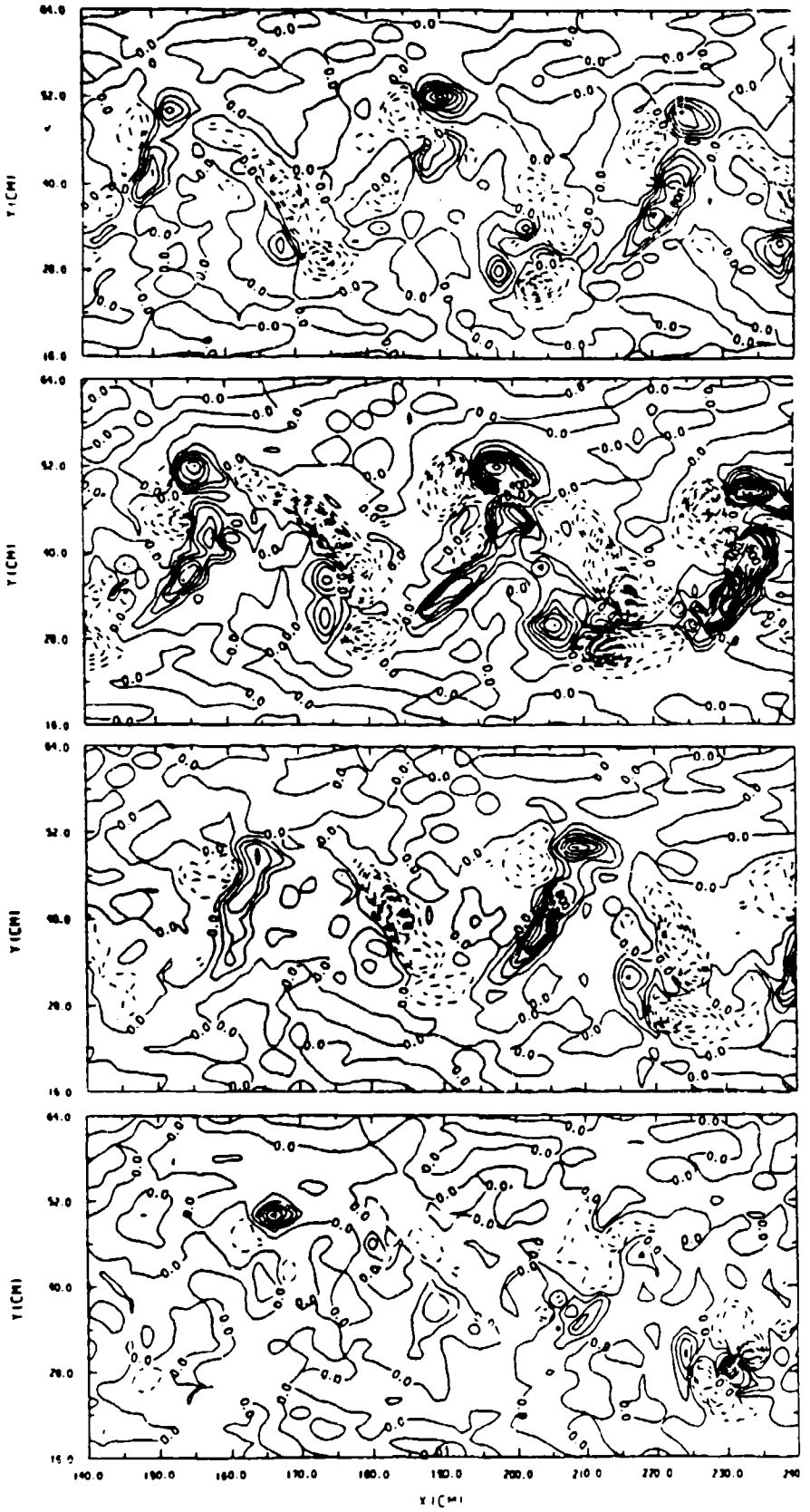

Figure 13. Continued.

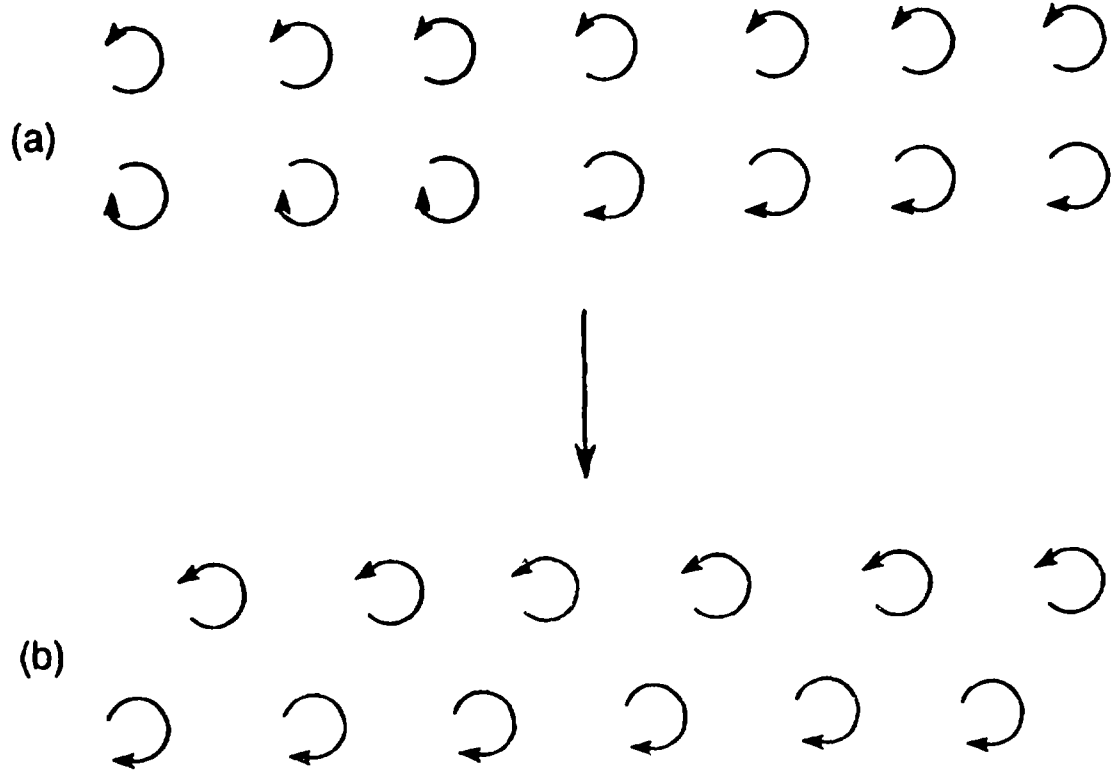

Figure 14. Transition of two rows of aligned and isolated vortices to gain stability.